Intercalibration of Boreal and Tethyan time scales: the magnetobiostratigraphy of the Middle Triassic and the latest Early Triassic from Spitsbergen, Arctic Norway

Mark W. Hounslow,[1] Mengyu Hu,[1] Atle Mørk,[2,6] Wolfgang Weitschat,[3] Jorunn Os Vigran,[2] Vassil Karloukovski[1] & Michael J. Orchard[5]

1 Centre for Environmental Magnetism and Palaeomagnetism, Geography, Lancaster Environment Centre, Lancaster University, Bailrigg, Lancaster, LA1 4YQ, UK
2 SINTEF Petroleum Research, NO-7465 Trondheim, Norway
3 Geological-Palaeontological Institute and Museum, University of Hamburg, Bundesstrasse 55, DE-20146 Hamburg, Germany
5 Geological Survey of Canada, 101-605 Robson Street, Vancouver, BC, V6B 5J3, Canada
6 Department of Geology and Mineral Resources Engineering, Norwegian University of Sciences and Technology, NO-7491 Trondheim, Norway

Keywords
Ammonoid biostratigraphy; Boreal; conodonts; magnetostratigraphy; Middle Triassic.

Correspondence
Mark W. Hounslow, Centre for Environmental Magnetism and Palaeomagnetism, Geography, Lancaster Environment Centre, Lancaster University, Bailrigg, Lancaster, LA1 4YQ, UK. E-mail: m.hounslow@lancs.ac.uk

doi:10.1111/j.1751-8369.2008.00074.x

Abstract

An integrated biomagnetostratigraphic study of the latest Early Triassic to the upper parts of the Middle Triassic, at Milne Edwardsfjellet in central Spitsbergen, Svalbard, allows a detailed correlation of Boreal and Tethyan biostratigraphies. The biostratigraphy consists of ammonoid and palynomorph zonations, supported by conodonts, through some 234 m of succession in two adjacent sections. The magnetostratigraphy consists of 10 substantive normal—reverse polarity chrons, defined by sampling at 150 stratigraphic levels. The magnetization is carried by magnetite and an unidentified magnetic sulphide, and is difficult to fully separate from a strong present-day-like magnetization. The biomagnetostratigraphy from the late Olenekian (Vendomdalen Member) is supplemented by data from nearby Vikinghøgda. The early and middle Anisian has a high sedimentation rate, comprising over half the ca. 140-m thickness of the Botneheia Formation, whereas the late Anisian and lower Ladinian is condensed into about 20 m. The two latest Boreal Ladinian ammonoid zones are absent as a result of erosional truncation below the Tschermakfjellet Formation. Correlation with Tethyan biomagnetostratigraphies shows the traditional base of the Boreal Anisian (base of the Grambergia taimyrensis Zone) precedes the base of the Anisian (using definitions based on the Dęsli Caira section in Romania). The Boreal upper Anisian Gymnotoceras rotelliforme and Frechites nevadanus ammonoid zones correlate with most of the Tethyan Pelsonian and Illyrian substages. The base Ladinian defined in the Tethyan global boundary stratotype and point (GSSP) is closely equivalent to the traditional base of the Boreal Ladinian at the Intornites oleshkoi Zone. The latest Olenekian—early Anisian magnetic polarity time scale is refined using the Spitsbergen data.

High-resolution correlation and chronostratigraphy is increasingly demanded for solving problems such as understanding palaeoclimatic and faunal changes on a global scale, defining stage boundaries, understanding and modelling basin evolution, and for many other purposes. Such correlations are problematic in the Mesozoic, as low-latitude and high-latitude faunas and floras were often very different, and hence often limit the use of biostratigraphy for global correlation. Tools of physical stratigraphy (such as magnetostratigraphy, sequence stratigraphy, cyclostratigraphy and chemostratigraphy) potentially provide higher resolution, but often need to be calibrated against conventional biostratigraphy to test their true utility. This work tests the relationship between the Boreal and Tethyan ammonoid biostratigraphies, by using the pattern of reverse to normal polarity changes

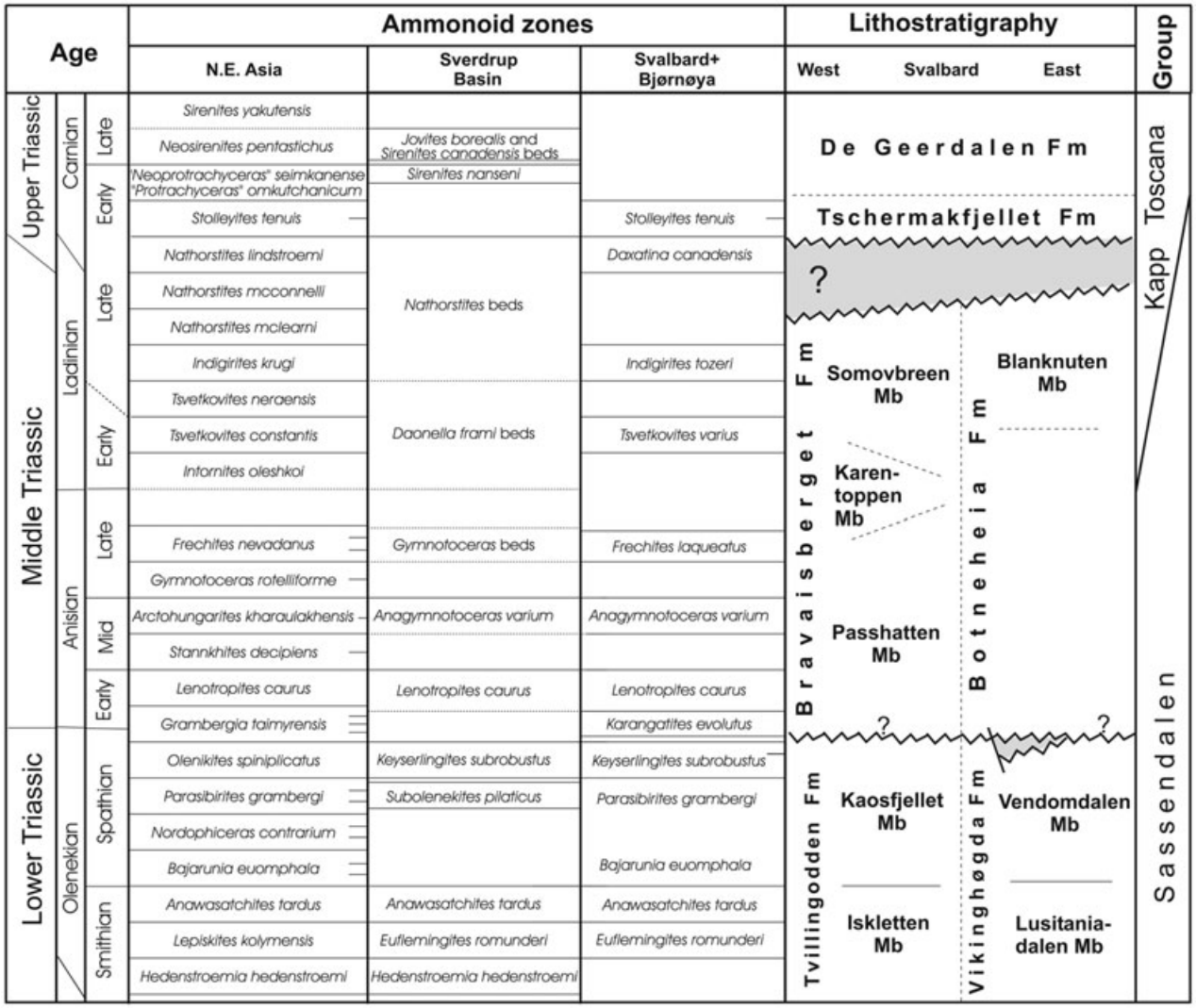

Fig. 1 Lithostratigraphy and ammonoid biostratigraphy of Svalbard and other key Boreal areas. Ammonoid biozones from Dagys & Weitschat (1993), Tozer (1994) and Dagys & Sobolev (1995).

gained from magnetostratigraphy as a cross-calibration tool with published biomagnetostratigraphies for the Middle Triassic (Muttoni et al. 1998; Muttoni et al. 2000; Nawrocki & Szulc 2000; Muttoni et al. 2004). The most complete of these in low latitudes is constructed from a composite of many sections tied together by conodont and magnetostratigraphic correlations (Muttoni et al. 2000; Muttoni et al. 2004). In contrast, this work utilizes a continuous succession from the latest Lower Triassic (Spathian) to the upper parts of the Middle Triassic (late Ladinian).

The Lower and Middle Triassic of Svalbard

The Triassic geology of Svalbard and adjacent parts of the Barents Sea continental shelf (Fig. 1) have a regional lithostratigraphy, defined on the basis of outcrops of Triassic rocks in the Svalbard Archipelago, shallow stratigraphic cores and hydrocarbon exploration wells in the surrounding seas (Mørk, Dallmann et al. 1999). The Lower and Middle Triassic succession of Svalbard consists of fine-grained siliciclastics with a dominant sediment supply from the west, resulting in deposits of coastal and shallow marine sandstones and shales in western Spitsbergen, and shales and siltstones in basinal settings in central and eastern Spitsbergen, Barentsøya and Edgeøya (Figs. 1, 2). This sedimentary pattern continues southwards under the Barents Sea, with the deposition of shales in basins and coarser grained clastics along the basin margins and local highs. Within eastern and central Spitsbergen, the Sassendalen Group is divisible into the Vikinghøgda and Botneheia formations (Mørk, Dallmann

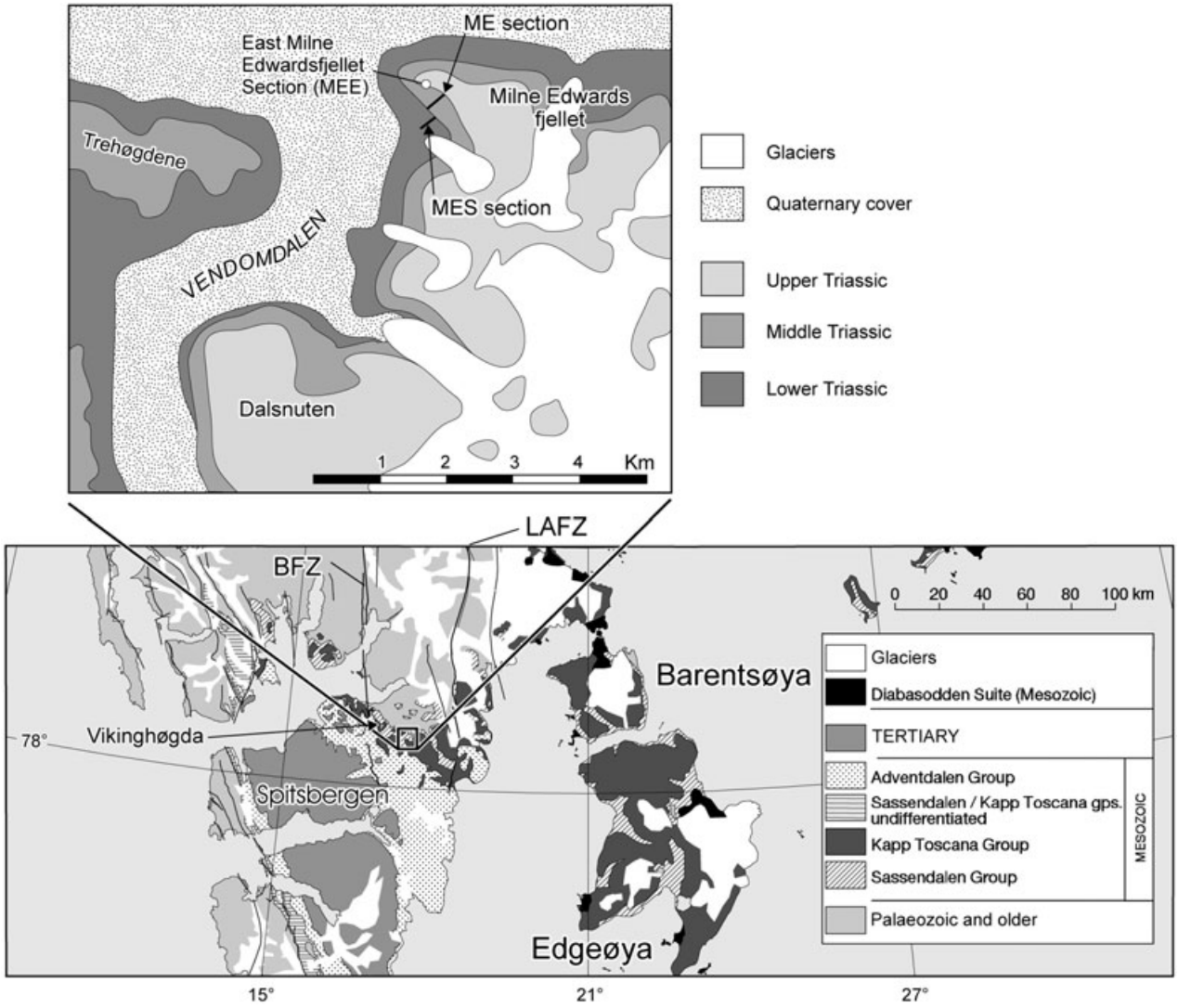

Fig. 2 Location map of Milne Edwardsfjellet in central Spitsbergen, and a simplified geology of southern Svalbard (modified from Dallmann 1999). There are separate legends for the main map and the inset. Abbreviations: BFZ, Billefjorden Fault Zone; LAFZ, Lomfjorden–Argardbukta Fault Zone. The inset shows the location of the sections at Milne Edwardsfjellet (MES, ME sections), and the MEE section described by Hounslow, Hu et al. (2007).

et al. 1999), which span the Lower and Middle Triassic (Fig. 1). The Lower and Middle Triassic possess sporadic Olenekian, Anisian and Ladinian ammonoid faunas, which can be closely related to richer and more complete ammonoid faunas in north-east Asia and British Columbia (Weitschat & Dagys 1989; Dagys & Weitschat 1993; Dagys & Sobolev 1995; Fig. 1). In contrast to ammonoids, the palynology from the Triassic in Svalbard and cores from the Barents Sea provide mostly continuous recovery, resulting in concurrent range zonations that have been dated by the co-occurring ammonoids (Hochuli et al. 1989; Vigran et al. 1998).

Section details

The biomagnetostratigraphy of two sections on the southern flanks of Milne Edwardsfjellet, referred to as the MES (from 78.2169° N, 17.5019° E to 78.2186° N, 15.5183° E) and ME sections (from 78.2169° N, 17.5025° E to 78.2183° N, 17.5169° E), are documented in Figs. 2 and 3. Additional sections to the west at Milne Edwardsfjellet (MEE section) have been described by Hounslow, Hu et al. (2007) from the uppermost part of the Botneheia Formation (Fm.) to the lowest beds of the overlying Tschermakfjellet Fm., and also through the entire Lower

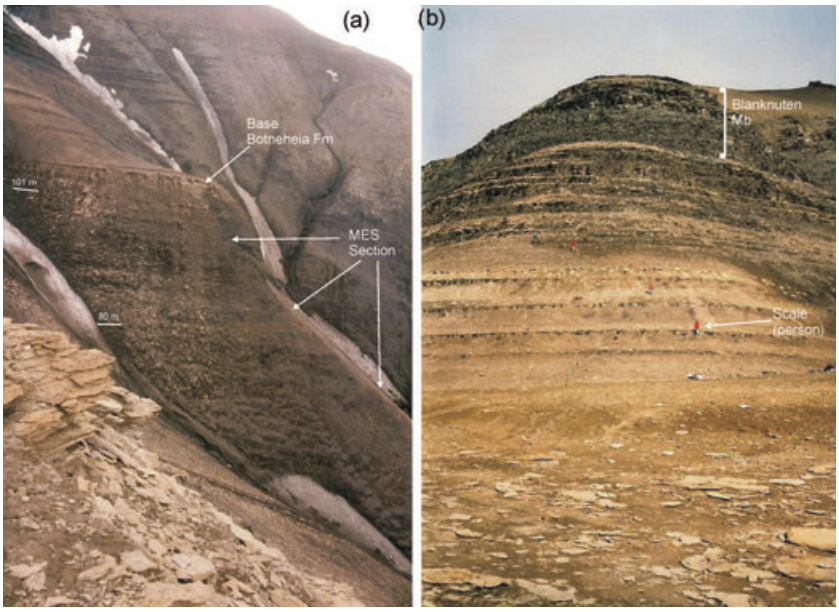

Fig. 3 (a) The uppermost part of the Milne Edwardsfjellet section MES (Vendomdalen Member). The top-most part of the ledge in the middle distance is the base of the Botneheia Formation (Fm.), overlying the top of the Vendomdalen Member (Mb.). The more easily weathered softer shales in the base of the Botneheia Fm. overlie this. The scale relates to Fig. 4a. (b) The Milne Edwardsfjellet section ME; the photograph was taken from near the base of the Botneheia Fm. The darker, steep cliff-forming units are the Blanknuten Mb., near the top of the formation.

Triassic at Vikinghøgda (Fig. 2; Mørk, Elvebakk et al. 1999; Hounslow et al. 2008).

The region around Vendomdalen is within the north-east part of the Central Tertiary Basin of southern Spitsbergen, and is structurally bounded to the west by the Billefjorden Fault Zone (BFZ), and to the east by the Lomfjorden—Argardbukta Fault Zone (LAFZ), which is a structural unit refered to as the Ny Friesland Block (Fig. 2). This block shows evidence of inversion during the Early Tertiary that was synchronous with folding in western Spitsbergen (Haremo & Andresen 1992).

The Vendomdalen Member (Mb.) consists of silty dark-grey laminated mudstone, with silty yellow-weathering diagenetic (ferroan) dolomite beds and nodules (Fig. 4). A shift from grey to dark-grey mudstone takes place at the lower boundary with the underlying Lusitaniadalen Mb. Dolomitic nodules and beds, some of them septarian, are up to ca. 30 cm in thickness. The upper part of the member forms a pronounced dolomitic siltstone cliff approximately 5 m thick (Figs. 3a, 4a). The top of the cliff is formed by a bioturbated bed, of between 0.5 and 1 m in thickness, which contains abundant phosphate nodules. This bed is regarded as part of the Botneheia Fm. The immediately overlying shales also contain abundant phosphate nodules.

The Botneheia Fm. consists of bituminous shales and mudstones, with occasional siltstones (forming steps in the hillside; Fig. 3b). It is divided into a lower unit of relatively soft shales, overlain by an upper unit of cliff-forming shales: the Blanknuten Mb. (Figs. 3b, 5a). The middle part of the Botneheia Fm. contains several carbonate-cemented siltstone beds that continue throughout the observable exposure (Fig. 3b). Phosphate, often in the form of nodules, is abundant both in these beds and in the interbedded shales (Fig. 5), attesting to a period of high organic productivity. The unit also has minor carbonate concretions, and layers of phosphatic and yellow-weathering dolomitic layers in the upper part of the unit. Thin limestone beds at ca. 100-m level and upwards, are dominated by minute bivalve shells forming coquina beds with *Tasmanites* algae (Fig. 5a).

The complete Botneheia Fm. appears to be exposed at Milne Edwardsfjellet, but the upper part of the formation in the ME section is disturbed by a regional décollement (Andresen et al. 1992). The uppermost 18 m of the Botneheia Fm. is better exposed, and is without structural disturbance at the MEE section to the west, as described by Hounslow, Hu et al. (2007). The décollement formed during the Palaeocene/Eocene, and was synchronous with more severe folding in western Spitsbergen (Haremo & Andresen 1992).

Methods

In total, 150 palaeomagnetic sample levels were collected through the succession (33 horizons were collected from the MES section, and 117 horizons were collected from the ME section), from concretionary calcite and dolomitic beds often in the Vendomdalen Mb., and occasionally from the Botneheia Fm. The intervening shale lithologies in the Vendomdalen Mb. were often too heavily fractured (i.e., were reduced to 1–2-cm-thick shale pieces) to collect oriented samples that could be measured. Samples from the Botneheia Fm. are mostly from mudstones and

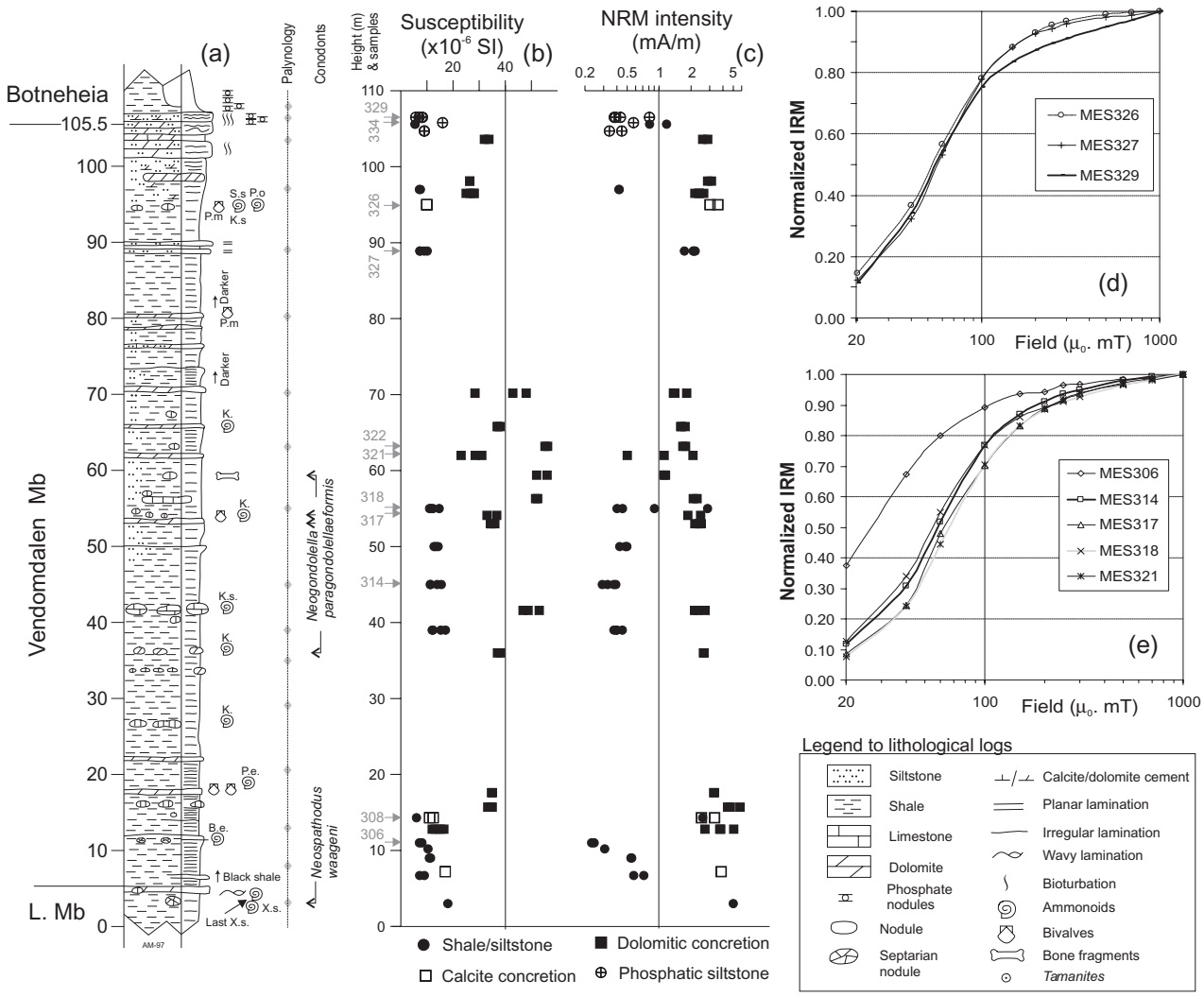

Fig. 4 Summary of the Milne Edwardsfjellet section MES through the Vendomdalen Member (Mb.). (a) Lithological log, biostratigraphy and palynostratigraphic sampling levels. (b, c) Magnetic properties of specimens. (d, e) Representative isothermal remanent magnetization curves. The positions of the samples illustrated and discussed in the text are marked (MES numbers) next to the magnetic susceptibility column in (b). Fauna codes: B.e., *Bajarunia euomphala*; K., *Keyserlingites* sp.; K.s. *Keyserlingites subrobustus*; P.e., *Parasibirites* cf. *elegans*; P.m., *Posidonia mimer*; P.o., *Popovites occidentalis*; S.s., *Svalbardiceras spitzbergensis*; X.s., *Xenoceltites subevolutus*. L. Mb.: Lusitaniadalen Mb.

shales, and from lower in the formation from a few siltstone beds. In both sections, bedding dips are of ca. 3° in a south-east direction. The samples were predominantly oriented blocks, although in the harder and more suitable lithologies the samples were collected by a water-cooled field drilling device. Samples were orientated using a dip meter and a magnetic compass.

In all, 292 specimens were demagnetized. Both thermal demagnetization and alternating demagnetization was used, using either a Magnetic Measurements Ltd. thermal demagnetizer (Aughton, Lancashire, UK) or a Molspin alternating field (AF) demagnetizer (Molspin Ltd, Newcastle on Tyne, UK). A composite demagnetization scheme using thermal demagnetization to 200–350°C (dictated by lithology), followed by AF demagnetization (to ca. 70–100 mT), was found to be most effective. Above a critical temperature (i.e., above ca. 250°C), the samples often showed large changes in mineralogy (large susceptibility and intensity increases), which limited any useful additional information obtained by thermal demagnetization; hence, AF demagnetization was used above this critical temperature to better isolate the Triassic magnetization. At most horizons at least two specimens were measured from each level. The specimens were measured on a CCL GM400 3-axis cryogenic magnetometer (noise level ca. 0.002 mA m^{-1}). Characteristic

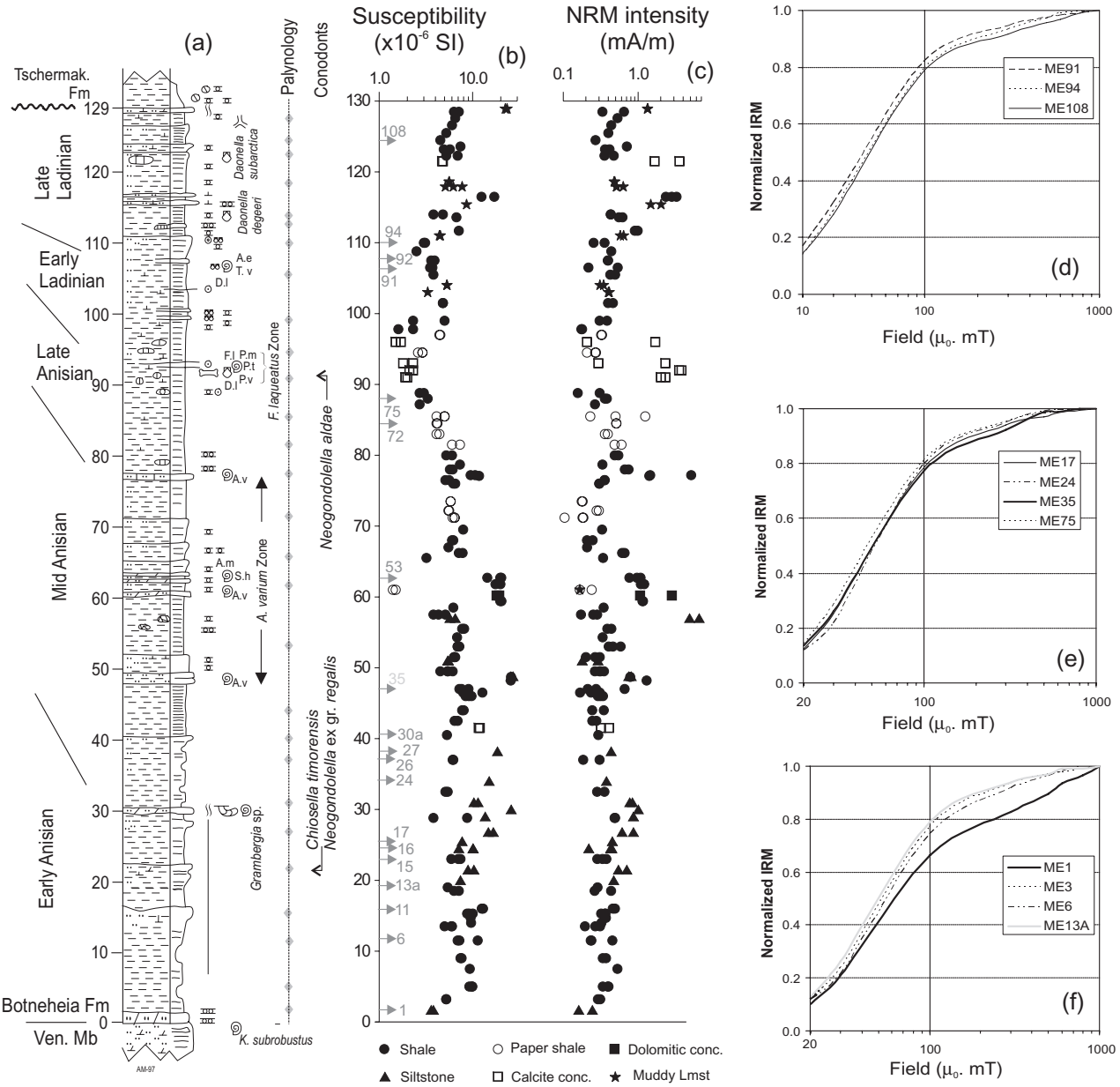

Fig. 5 Summary of the Milne Edwardsfjellet section ME from the Botneheia Formation (Fm.). (a) Lithological log, biostratigraphy and palynostratigraphic sampling levels. (b, c) Magnetic properties of specimens. (d–f) Representative isothermal remanent magnetization curves. The positions of the samples illustrated and discussed in the text are marked (ME numbers) next to the magnetic susceptibility column in (b). Fauna codes: A.e., *Aristoptychites euglyphus*; A.m., *Amphipopanoceras* cf. *medium*; A.v., *Anagymnotoceras varium*; D.l., *Daonella lindstroemi*; F.l., *Frechites laquatus*; P.m., *Parafrechites migayi*; P.t., *Aristoptychites trochleaeformis*; P.v., *Parapopanoceras malmgreni*; S.h., *Stannkhites hayesi*; T.v., *Tsvetkovites varius*. Also see key to lithological log in Fig. 4.

remanent magnetisation (ChRM) directions were isolated using principle component analysis, as implemented in LINEFIND (Kent et al. 1983). Both linear trajectory and great circle analysis have been used to define the palaeomagnetic behaviour.

Considering the dominance of pyrite-bearing organic-rich shale and siltstone in the formations, there was an expectation that magnetic sulphides (greigite and pyrrhotite) might make a significant contribution to the magnetization, and so suitable tests were performed to try to identify these. Progressive isothermal remanent magnetization (IRM), up to 1 T, was applied to a representative subset of specimens, to investigate the coercivity behaviour. Thermal demagnetization of a three-

component IRM was used to investigate the blocking and alteration temperature behaviour (Lowrie 1990). Magnetization—temperature behaviour at low temperatures (measured using a Princeton Measurements Corporation Magnetic Property Measurements System; Princeton, NJ, USA) was used to test for magnetite and pyrrhotite structural transitions.

Samples for palynology were collected in parallel with the magnetostratigraphy. These were preferentially collected from shale units interbedded in the sequence, and were processed using standard techniques in the SINTEF laboratory. A subset of samples, at selected palaeomagnetic sampling horizons, were processed for conodonts at the Geological Survey of Canada (Vancouver).

Ammonoid and conodont biostratigraphy

At the base of the MES section, the ammonoid *Xenoceltites subevolutus* occurs in the uppermost part of the Lusitaniadalen Mb. (Fig. 4a). A parallel section a few tens of metres to the east contains the ammonoids *Anawasatchites* sp., *Arctoprionites nodosus*, *X. subevolutus*, *Anasibirites* sp., *Tellertites furcatus* and *Pseudosageceras* sp. at the same level, indicating the latest Smithian Anawasatchites tardus Zone (Figs. 1, 4). A conodont collection from the 3-m level (in the Lusitaniadalen Mb.; Fig. 4) comprises *Neospathodus waageni*, which is a Smithian index species (Sweet 1970).

The presence of the Bajarunia euomphala Zone of early Spathian age is indicated by the occurrence of the zonal fossil *B. euomphala* at approximately 11.2 m above the base (Fig. 4a). Above this, a thin Parasibirites grambergi Zone (middle Spathian) is indicated by the ammonoid *Parasibirites* cf. *elegans* (Dagys & Sobolev 1995).

The major part of the Vendomdalen Mb. is latest Spathian, corresponding to the Keyserlingites subrobustus Zone, based on occurrences of *Keyserlingites* sp. starting from the 26-m level (Fig. 4a). In the section some 15 m below the top of the Vendomdalen Mb., a diverse fauna of the ammonoids *Svalbardiceras spitzbergensis*, *K. subrobustus*, *Popovites occidentalis*, *Monacanthites monceros*, *Procarnites* cf. *modestus*, *Arctomeekoceras* sp. nov., and *Pseudosageceras* sp. nov., and the bivalve *Posidonia aranea*, occurs. A similar section, a few tens of metres to the east (visible in Fig. 3), displays the same fauna some 20 m below the top of the Vendomdalen Mb. Here, *K. subrobustus* occurs in the cliff just below the base of the Botneheia Fm. (Fig. 4a). This fauna belongs to the latest Spathian Keyserlingites subrobustus Zone, and *S. spitzbergensis* indicates the youngest subzone of the Siberian Olenekian (Dagys & Sobolev 1995).

Four conodont collections were recovered from the Vendomdalen Mb. at the 26-, 53- and 59.4-m levels (Fig. 5a). Each contains neogondolellids, some of which resemble the species *Columbitella*? sp. nov. K, and the Siberian species *Columbitella*? *paragondolellaeformis*, described from the latest Olenekian of Siberia (Dagis 1984; Klets 1998; Nakrem et al. 2008 [this issue]).

The macrofossil content of the ME section is relatively sparse, and fossils were collected along wide exposures, and were correlated with the measured section laterally (Fig. 5a). The first extensive dolomitic siltstone beds contain the ammonoid *Grambergia* sp., of early Anisian age (Fig. 5), without direct evidence of the earliest Anisian in the section. Nevertheless, the ammonoid *Karangatites evolutus* occurs within the lowest 1 m of the Botneheia Fm. at Wallenbergfjellet (northern side, some 9.4 km to the NNE), equating with the second ammonoid subzone of the Grambergia taimyrensis Zone, indicating the earliest Anisian is probably present in the sections from the eastern Sassendalen region. This is supported by a sample from the 21.5-m level, which contains the conodonts *Chiosella* cf. *timorensis* and *Neogondolella* ex. gr. *regalis*, which also imply an early Anisian age (Orchard et al. 2007).

The middle part of the unit (Fig. 5a) contains the ammonoids *Amphipopanoceras* cf. *medium*, *Stannakhites hayesi*, *Anagymnotoceras varium*, *Hollandites* sp. and *Leiophyllites* sp. nov., which are all of Middle Anisian age. Late Anisian beds are indicated by the ammonoids *Frechites laqueatus*, *Aristoptychites trochleaeformis*, *Parapopanoceras malmgreni* and *Parafrechites migayi*, and by the bivalve *Daonella lindstroemi*. The ammonoids *Aristoptychites euglyphus*, *Tsvetkovites varius* and *Ussurites* sp., and the bivalve *D. lindstroemi*, are indicators of Early Ladinian age (Fig. 5). A conodont collection from the 91-m level contains elongate representatives of the *Neogondolella constricta* group, which can most closely be assigned to *Neogondolella aldae* (*sensu* Orchard & Tozer 1997), suggesting a latest Anisian to early Ladinian age (from the Frechites chischa Zone to the Tuchodiceras poseidon Zone of the British Columbia ammonoid zones). Hence, in comparison with the early and middle Anisian, the late Anisian and early Ladinian intervals appear to be distinctly condensed.

No ammonoids were found in the uppermost part of the ME section, but both the bivalves *Daonella subarctica* and *Daonella degeeri* are of Late Ladinian age (Weitschat & Dagys 1989). The MEE section to the west contains the ammonoid *Indigirophyllites spetsbergensis* with *Protrachyceras* sp., along with the bivalve *D. subarctica*, 13 m below the top of the Botneheia Fm. Two conodont productive levels occur in the MEE section: one in the top 0.2 m of the Botneheia Fm., and the second 1 m into the Tschermakfjellet Fm. (Hounslow, Hu et al. 2007). Both these levels are dominated by the conodont *Neogondolella liardensis*, which in British Columbia commonly occurs

through the Frankites sutherlandi and Trachyceras desatoyense zones, co-occurring with *Daxatina* sp. (Orchard 2007). The upper level also contains *Metapolygnathus* ex. gr. *polygnathiformis* and *Metapolygnathus* cf. *lobatus*, with the former having a more limited range in these same two ammonoid zones.

Palynology

The palynology is significant for three reasons. Firstly, the other biostratigraphic and magnetostratigraphic data from the sections provides independent assessment of the age range of relevant miospores. Secondly, by comparison with the assemblage zones constructed by Hochuli et al. (1989) and Vigran et al. (1998), and with their associated ammonoid age control (Fig. 6), the palynostratigraphy allows some additional age constraints in the sections. Thirdly, the palynology provides a more continuous record of stratigraphic change through the sections than the conodont and macrofossil data.

Like other Triassic outcrops on Svalbard, the palynofloras from the sections are not as diverse as those from cores in the Barents Sea, as detailed in the discontinuous Svalis Dome cores (Fig. 6; Vigran et al. 1998). The lack of diversity is probably a reflection of outcrop weathering. Consequently, it is not possible to assign all of the assemblages from outcrops to the diverse Svalis assemblages, and so a mix of assemblages from Hochuli et al. (1989) and Svalis assemblages are used here (Fig. 6).

Vikinghøgda Formation

The Vikinghøgda Fm. is dominated by a rather monotonous flora of pollen and spores. Bisaccate pollen comprises alete indeterminate forms and taeniate forms, such as *Lunatisporites*; monolete pollen includes the *Pretricolpipollenites* and *Cycadopites* groups. The trilete spores are dominantly smooth forms, and small cavate ones like *Densoisporites nejburgii*. The dominant plankton is represented by leiospheres, tasmanitids and *Micrhystridium*.

The single sample from the Lusitaniadalen Mb. is dominated by cavate spores of *Punctatisporites* spp. and other smooth triletes (Fig. 7). There are rare *Kraeuselisporites*, but little bisaccate pollen, although fungal remains, type 1 (Hochuli et al. 1989), are common. In view of its low diversity, this association can be regarded as equivalent to assemblage N of Hochuli et al. (1989). Spores in the richer association, at the same level at Vikinghøgda (Mørk, Elvebakk et al. 1999), allow correlation with assemblage Svalis-2 of Vigran et al. (1998), which in these locations occurs with ammonoids indicative of the Anawasatchites tardus Zone.

In the lowest part of the Vendomdalen Mb. (8.0–12.8-m levels at Milne Edwardsfjellet; Fig. 7), the indeterminate and taeniate bisaccate pollen *Pretricolpipollenites* sp. and *Cycadopites* spp. occur together with the common-to-dominant cavate spores (Fig. 7), features that indicate the assignment of these levels to assemblage M of Hochuli et al. (1989). The 20.5–70.2-m interval in the MES section dominantly contains bisaccates, *Cycadopites*, *Pretricolpipollenites* and cavate spores, with the closest resemblance (based on relative characteristics) being to assemblage L (Fig. 6). In the youngest parts of the Vendomdalen Mb. (at the 80.2-m level), *Jerseyiaspora punctispinosa*, which defines the base of the Svalis-4 assemblage (Figs. 6, 7), is associated with the introduction of spores like *Retusotriletes* sp. and the common *Gordonispora fossulata* (Vigran et al. 1998).

Botneheia Formation

The basal layers of the Botneheia Fm. at Milne Edwardsfjellet (MES section, at the 106.5-m level) are distinguished by a poorly preserved, low diversity and non-diagnostic association of palynomorphs, dominantly *Micrhystridium* spp. (Fig. 7), with an association tentatively considered as equivalent to assemblage L. The presence of *Vittatina* spp. and *Nuskoisporites* sp. (both restricted to the Permian) indicates reworking at the 108.0-m level.

The succession of samples from the Botneheia Fm. in the ME section may be divided into two major intervals, both dominated by bisaccate pollen and diverse acritarchs. Between the 1.7- and 53.0-m levels, there are low numbers of spores that show some diversity (Fig. 7). Between the 61.0- and 127.6-m levels, spores are rare (Fig. 7).

The consistent presence of *D. nejburgii*, together with *Triadispora labichensis*, *Acanthotriletes* sp. F (Vigran et al. 1998), *Accinctisporites circumdatus*, *Cordaitina minor* and *Illinites chitonoides*, allows the assignment to assemblage Svalis-5, which is similar to assemblage L in its upper range (Figs. 6 and 7; Hochuli et al. 1989). The interval 40.0–53.0 m contains *Conbaculatisporites hopensis*, *Striatella seebergensis*, *Jerseyiaspora punctispinosa* and *Lueckisporites junior*, which allows recognition of assemblage Svalis-6.

Fig. 6 Key miospore ranges that define the palynostratigraphy in the zonations of Hochuli et al. (1989) from Svalbard and the Barents Sea, and from Vigran et al. (1998) for the Svalis Dome cores. The associated ammonoids, which date the zonations, are those indicated by Hochuli et al. (1989) and Vigran et al. (1998). The miospore species and genera indicated in bold are key markers used in defining the assemblage zones. Triassic stage assignment for the Svalis Dome zonation is in part based on this work.

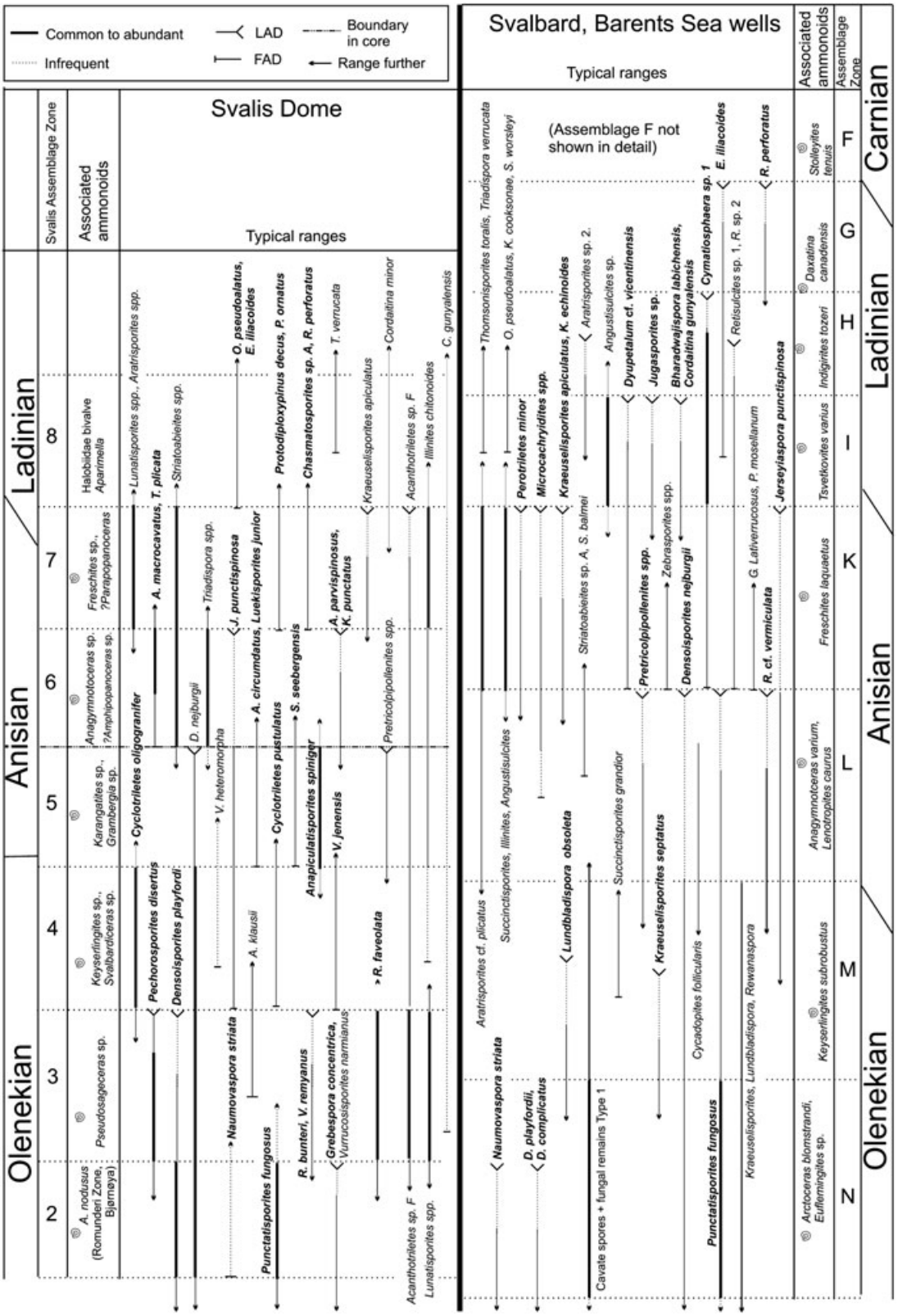
Olenekian
Anisian
Ladinian
Svalis Assemblage Zone
Associated ammonoids
Svalis Dome
Typical ranges
Common to abundant
Infrequent
LAD
FAD
Boundary in core
Range further
Svalbard, Barents Sea wells
Typical ranges
(Assemblage F not shown in detail)
Associated ammonoids
Assemblage Zone
Olenekian
Anisian
Ladinian
Carnian

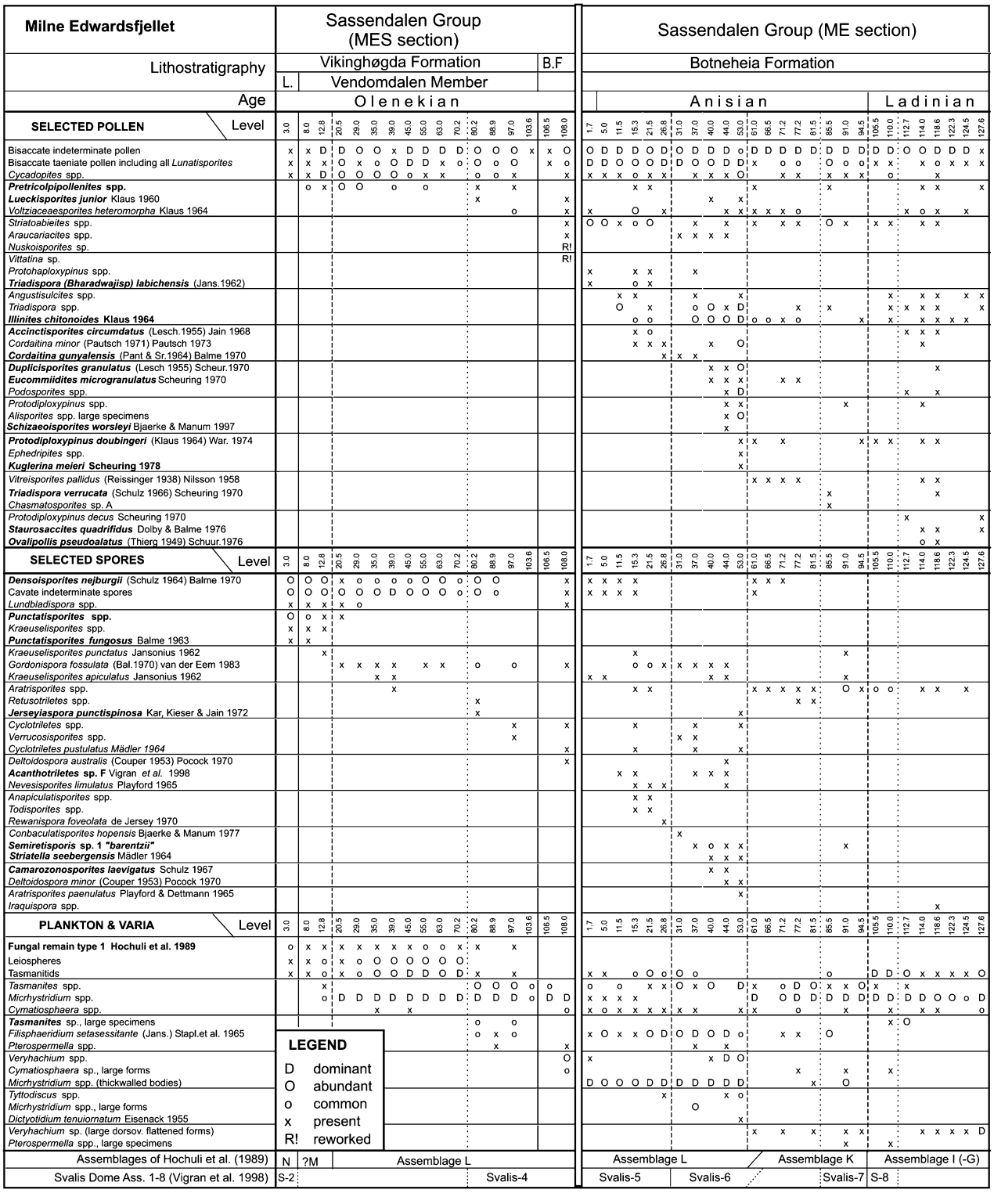

Fig. 7 Palynology of the Milne Edwardsfjellet sections. See Figs. 4 and 5 for the location of the samples. Miospores indicated in bold are of stratigraphic significance for correlation. *Striatoabieites* and *Triadispora* taxa have been presented as groups. B.F., Botneheia Formation (Fm.); L., Lusitaniadalen Member (Mb.). Stage assignment based on this work.

The Svalis-6 assemblage in the ME section includes forms that, according to Vigran et al. (1998), have their earliest appearance in the late Anisian and early Ladinian assemblages at the Svalis Dome, i.e., *Eucommiidites microgranulatus* in Svalis-7, and *Camarozonosporites laevigatus*, *Duplicisporites granulatus*, *Kuglerina meieri*, *Protodiploxypinus doubingeri*, *Schizaeoisporites worsleyi* and *Semiretisporis* sp. 1 in Svalis-8. Clearly, our understanding of palynomorph ranges in the Boreal realm is incomplete, a fact that can also be deduced from the Russian data in Mørk et al. (1992).

At the 61.0-m level and above, the dominance of bisaccate pollen, along with the introduction of large specimens of *Veryhachium*, reflects an environmental change that is coincident with the increased abundance of phosphate (Fig. 5a). The presence of *D. nejburgii* up to the 71.2-m level could indicate that the Svalis-6 assemblage might extend to this level. However, these spores are considered to represent reworking. *Chasmatosporites* sp. A and *Triadispora verrucata* at the 85.5-m level are interpreted as evidence for the Svalis-7 assemblage (Fig. 7).

Between the levels at 112.7 and 114.0 m, there is an increase of pollen diversity, and the earliest records of *Protodiploxypinus decus*, *Ovalipollis pseudoalatus* and *Staurosaccites quadrifidus* allow the recognition of this association as the Svalis-8 assemblage. A similar assemblage in the youngest part of the Botneheia Fm. in the MEE section (co-occurring with ammonoids of the Indigirites tozeri Zone; Hounslow, Hu et al. 2007), does not contain evidence for the distinction of younger Ladinian layers; hence, assemblage I (to G) of Hochuli et al. (1989) is interpreted for the uppermost layers of the Botneheia Fm. (Fig. 7).

Palaeomagnetic results and magnetic properties

Magnetic mineralogy

In the Vendomdalen Mb., magnetic susceptibility is generally some threefold larger in the dolomitic horizons in comparison with the non-dolomitic horizons (Fig. 4b). This may be because ferroan dolomite has an appreciably larger susceptibility than most clays and calcite (Rochette et al. 1992). The natural remanent magnetization (NRM) intensities are also strongly controlled by the lithology, with the dolomitic and calcitic concretions having significantly larger values, often exceeding 1 mA m^{-1}, in comparison with the shales and siltstones, which are often less than 1 mA m^{-1} (Fig. 4c). The IRM curves (Fig. 4d, e) demonstrate that there is not a consistent difference in remanence mineralogy or granulometry between these lithologies; hence, this lithology-related difference may be related to the better preservation of Fe oxides in the concretionary lithologies, as it is expected that sulphide diagenesis will have destroyed most of the originally deposited Fe oxides (Canfield & Berner 1987).

The magnetic susceptibility allows the subdivision of the Botneheia Fm. into three major intervals: a lower unit, from the 0- to 85-m levels, with elevated and slightly variable magnetic susceptibility; a unit with generally low susceptibility, from the 85- to ca. 100-m levels; and an interval, from the ca. 100- to 130-m levels, with values similar to those of lower in the section (Fig. 5b). The lowest 2 m of the formation also have lower values. These changes are probably related to a carbonate-rich interval between the 85- and 100-m levels, and to a phosphate-rich interval in the lowest 2–3 m. The diamagnetic carbonate (and phosphate) dilute the detrital material, which is likely to be responsible for the susceptibility. In the Botneheia Fm., like the underlying Vendomdalen Mb., the elevated NRM intensities of the samples seem to be mostly related to concretionary carbonate lithologies (Fig. 5c).

The IRM acquisition curves are similar for most samples from the Vendomdalen Mb. and Botneheia Fm. (Figs. 4, 5d–f), pointing to near saturation by 100–200 mT, with limited acquisition above 300 mT, indicating the remanence properties are dominated by low-coercivity phases (magnetite, or a magnetic sulphide).

The three-component IRM data from both the Vendomdalen Mb. and the Botneheia Fm. are similar, often showing an accelerated loss of remanence in all three coercivity fractions, most often starting at about 300°C, with little remanence persisting above 400–450°C (Fig. 8a). This seems to coincide with the start of mineralogical alteration, exemplified by the increase in susceptibility during heating (Fig. 7a). This behaviour may be attributable to greigite(?) oxidation during demagnetization (Dekkers et al. 2000), rather than to any expression of Curie or blocking temperature, as all three coercivity components show similar remanence loss (Fig. 8a).

The low-temperature measurements on both cooling and warming cycles shows a weak magnetite Verwey transition at about 120 K, and no evidence of the pyrrhotite magnetic transition at ca. 34 K (Fig. 8b; Hunt et al. 1995). The small loss of moment on crossing the magnetite Verwey transition (some 2% on cooling and 20% on warming) may result from either its fine grain size (<ca. 0.2 μm in diameter) or oxidation of the magnetite (King & Williams 2000), or from its low abundance.

In conclusion, the magnetic properties appear to be carried by both magnetite and magnetic sulphide (greigite?), without significant discrimination of these phases in terms of coercivity differences. It seem probable that the coercivities greater than 100–200 mT may be carried by greigite, rather than by "soft" haematite.

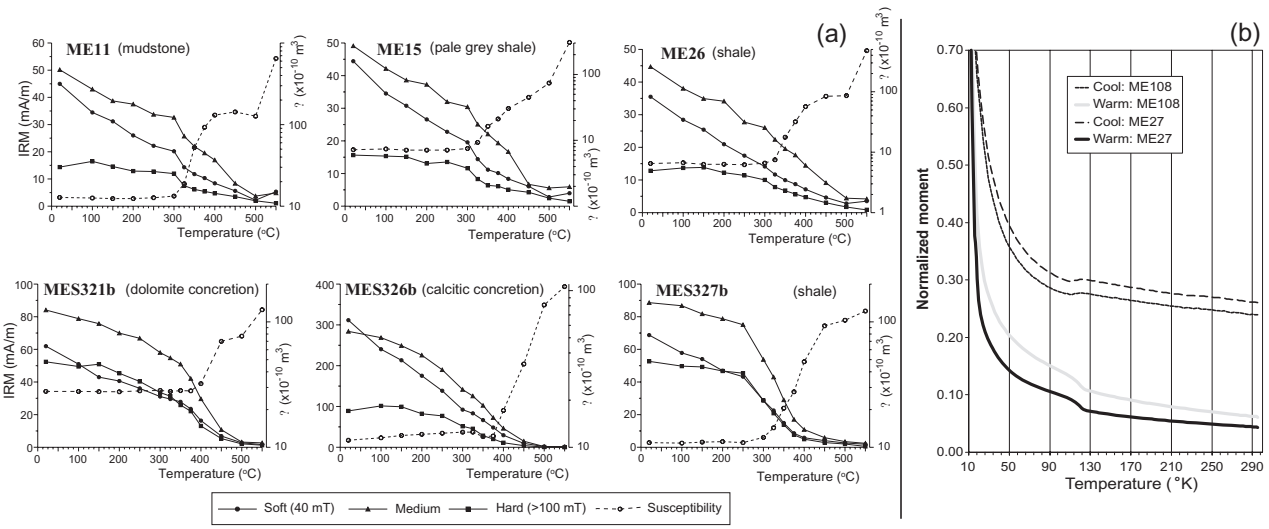

Fig. 8 (a) Thermal demagnetization of a three-component isothermal remanent magnetization (IRM) for representative samples from the Vendomdalen Member (Mb.) and the Botneheia Formation (Fm.). The stratigraphic locations of the specimens are shown in Figs. 4 and 5. (b) Low-temperature remanence measurements on two specimens, showing zero-field cooling of a room temperature 300-mT IRM, and warming of a 2.5-T IRM applied at 10 K (normalized to moment at 10 K). The stratigraphic locations of the specimens are shown in Fig. 5.

Palaeomagnetic behaviour

Thermal demagnetization above ca. 250–325°C often induced a large increase in susceptibility, without improvement in component identification. The most reliable demagnetization method was to clean with thermal demagnetization to 250–350°C (temperature partly dictated by lithology), prior to the heating-induced alteration, followed by AF demagnetization up to about 80–90 mT (Fig. 9).

The demagnetization of specimens produced two magnetization components. Firstly, there was often a steep, downwards directed, overprint magnetization, which was sometimes removed at lower AF demagnetization stages (<20 mT), but often persisted into the mid or later stages (40–70 mT) of AF demagnetization (Fig. 9a, b). The directional mean of this overprint component is notably displaced to the south for specimens interpreted to be of Triassic reverse polarity, compared with those of normal polarity (Fisher means; Dec/Inc/α_{95}/N_1: MES normal = 004°/81°/4.7°/41, MES reverse = 266°/75°/12.1°/23; MES normal = 013°/83°/3.3°/86; ME reverse = 199°/78°/5.2°/98; see Table 1 for terms). Hence, the overprint component is interpreted to be a composite: predominantly a Brunhes-age overprint, but combined with variable contributions from a Triassic dual-polarity magnetization (Fig. 9d, c). In 26 and 32% of specimens from the ME and MES sections, respectively, this composite magnetization direction persisted until complete demagnetization, without any evidence of a Triassic component.

Removal of this overprint revealed the ChRM component interpreted as a dual-polarity north-east and south-west directed Triassic magnetization (Fig. 9c, f). This was most often isolated above about the 40-mT AF demagnetization stage, and was predominantly isolated through the origin, although superimposed spurious instrument-derived magnetization often hindered lines-fitted through the origin (Fig. 9c). Some 28 and 23% of specimens from the MES and ME sections, respectively, had suitable linear trajectory line fits (here termed S-type data). The mean directions for the ChRM fitted-line data for the ME section pass the reversal test (McFadden & McElhinney 1990; Table 1). No reverse-polarity samples with S-type data were extracted from the MES section (Table 1; Fig. 10a). Some 40 and 51% of specimens from the MES and ME sections, respectively, displayed great circle trends of varying arc length towards the reverse- and normal-polarity directions interpreted as being Triassic in origin (here referred to as T-type demagnetization behaviour; Fig. 9a, d, e). These great circle paths were used with the fitted-line ChRM directions to determine the combined mean directions (McFadden & McElhinney 1988). These combined mean directions only pass the reversal test for the ME section (Table 1). The reversal test on the specimen data from the MES section fails the reversal test. There is no polarity bias in the data from the concretion levels sampled (Fig. 10a, b); although on average, samples from calcite concretions possess poorer palaeomagnetic behaviour than those from dolomite concretions.

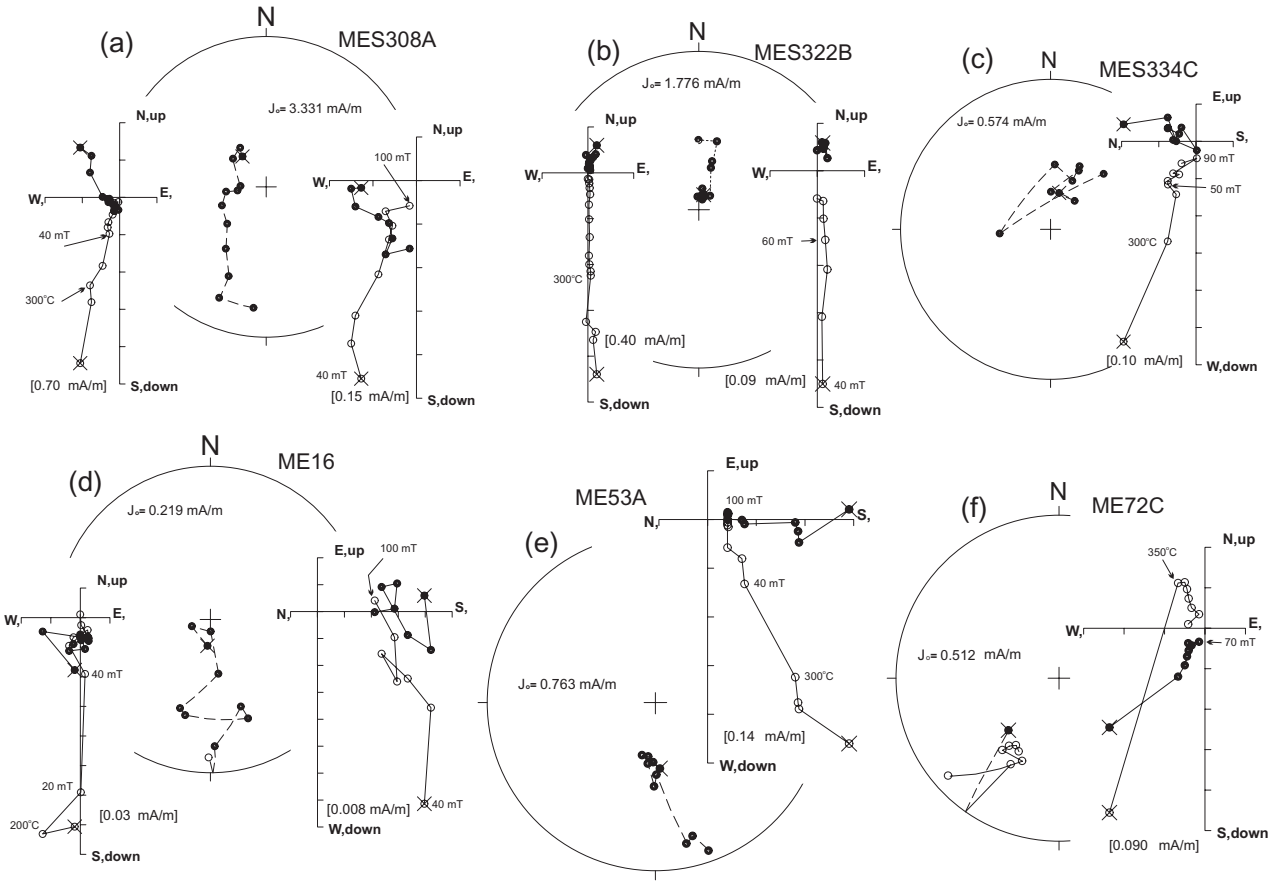

Fig. 9 Representative specimen demagnetization data. The stratigraphic locations of the specimens are shown in Figs. 4 and 5. Detail from the Zijderveld plots for (a), (b) and (d) is shown on the right of the stereonet in each case. (a) MES308A (14.3-m level; limestone nodule): demonstrates great circle type behaviour (demagnetization class T2), trending towards reverse polarity, after removing a north-west directed (323°, 62°) composite component. Great circle fitted between 200°C and origin, with pole at 101°, +19°. (b) MES322B (63.2-m level, dolomite nodule): illustrating removal of a steep present-day-like direction (347°, 83°, from 300°C to 60 mT), and isolation of an interpreted Triassic normal-polarity direction (016°, 66°) from 70 mT to the origin (demagnetization class S3). (c) MES334C (105.8-m level, phosphatic siltstone): shows the isolation of an interpreted Triassic normal polarity between 50 and 90 mT (032°, 56°, demagnetization class S2), after removal of a slightly steeper lower stability component (315°, 67°). (d) ME16A (24.5-m level, pale grey siltstone): demonstrates great circle behaviour (pole at 090°, 2°, demagnetization class T1) towards an interpreted reverse-polarity direction, up to 100 mT demagnetization. (e) ME53A (62.7-m level, cemented shale): shows great circle behaviour (pole at 059°, 18°, demagnetization class T2) towards an interpreted reverse polarity. The composite low-stability component has a fitted-line direction of 194°, 67° between 200°C and 100 mT. (f) ME72C (84.5-m level, paper shale): shows isolation of a fitted-line, the characteristic remanent magnetization (ChRM) direction (200°, –60°, demagnetization class S1) between 10 and 70 mT demagnetization. Numbers in brackets indicate the scale between ticks on the Zijderveld plots.

Table 1 Fisher means, reversal tests and virtual geomagnetic poles (VGPs).

	Dec.	Inc.	*K*	$\alpha 95$	N_l/N_p	Reversal test	G_O/G_C	P_{lat}	P_{long}	D_p/D_m
MES section (Vendomdalen Member)										
Line fitting	36.3	59.7	36.3	5.0	24/0	—	—	50	154	5.7/7.5
GC means	38.9	67.7	36.5	3.1	24/34	R-	15.7/6.5*	59	147	4.3/5.2
ME section (Botneheia Formation)										
Line fitting	45.3	61.9	31.3	3.7	48/0	Rc	16.9/31	50	143	4.6/6.0
GC means	39.3	71.1	25.1	2.3	48/105	Rb	8.1/8.8	64	144	3.5/4.0

K, Fisher's precision parameter; $\alpha 95$, Fisher's 95% cone of confidence. N_l is the number of specimens with fitted lines, and N_p is the number of specimens with great circle planes used to determine the mean direction. G_0 is the angular separation between the inverted reverse and normal directions, and G_c is the critical value for the reversal test. In the reversal test, the G_0/G_c values flagged with an asterisk indicate common *K* values; others not flagged have statistically different *K* values for reverse and normal populations, in which case a simulation reversal test was performed. P_{lat} and P_{long} are the latitude and longitude of the mean VGP. GC means are the great circle combined means. *Dp*/*Dm* is semi-axes of the ellipse of confidence (in degrees) parallel and perpendicular to the great circle connecting the sampling site and the VGP pole.

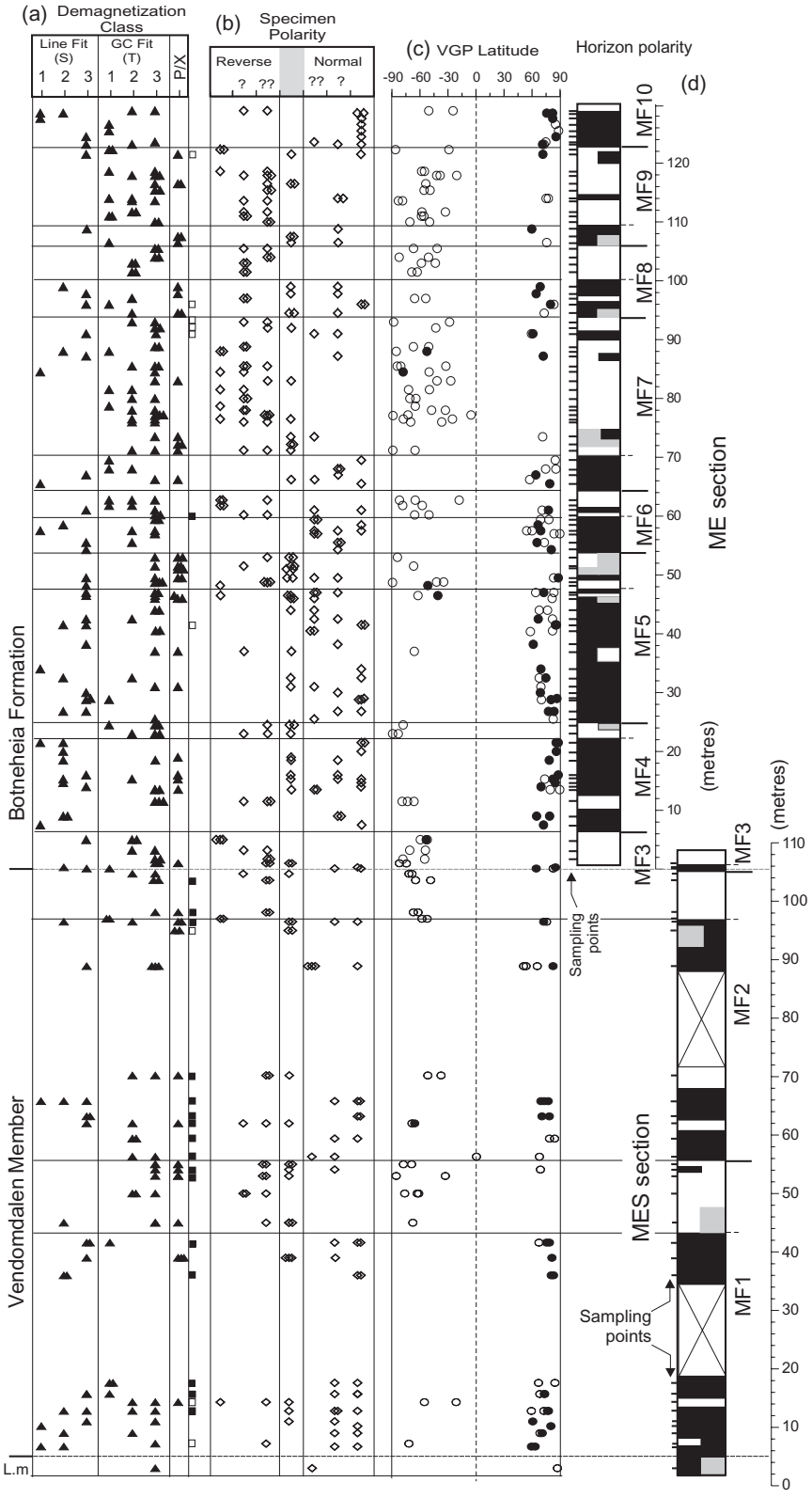

Fig. 10 Magnetostratigraphic data of the specimens. (a) Demagnetization behaviour showing categorization into: linear trajectory fitted-lines, from good (S1) to poor (S3); fitted great circles from good (T1) to poor (T3), and specimens with no (P/X) Triassic magnetization (see text for details). Squares on right-hand side of column indicate sample levels from dolomite (filled) and calcite (unfilled) concretions. (b) The interpreted specimen polarity quality; specimens in the middle grey column have not been assigned a polarity (?? denotes poorest quality for reverse and normal polarities). (c) The virtual geomagnetic pole (VGP) latitude, with filled symbols for specimens possessing an S-class characteristic remanent magnetization, and unfilled symbols for specimens with T-class great circle behaviour. (d) Horizon polarity: white, reversed polarity; black, normal polarity; grey, uncertain; half-bar width indicates a single useful specimen from this level.

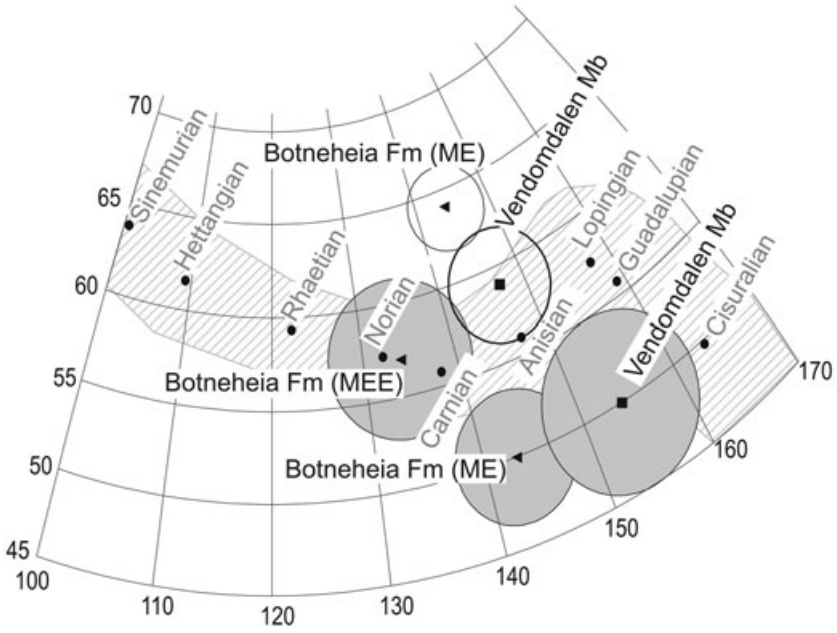

Fig. 11 Mean virtual geomagnetic poles (VGPs) with respect to the apparent polar wander path (APWP) for Baltica. Hatching indicates the 95% confidence swathe around the mean APWP (from Torsvik & Cocks 2005). Poles (filled circles) are marked in 10-My increments, using the time scale in the palaeomagnetic database. Fitted-line ChRM mean directions are indicated with grey 95% confidence ellipses; non-filled ellipses are the combined great circle and ChRM means from Table 1. Data for the Milne Edwardsfjellet MEE section, in the uppermost part of the Botneheia Formation (Fm.), are from Hounslow, Hu et al. (2007).

The great circle combined means are significantly steeper than the ChRM fitted-line only data (Table 1). We consider it possible that the great circle means may be unduly biased by directional contamination in the great circle data, from the Brunhes-age overprint. Hence, ChRM fitted-line data probably provide the best estimates of the mean Triassic magnetic field direction for the sample set. However, in terms of comparison with the Baltica apparent polar wander path (APWP), only the combined mean for the ME section falls outside of the 95% confidence swathe (Fig. 11). The confidence ellipses of the ChRM fitted-line means overlap the 95% confidence swathe of the Baltica APWP (Fig. 11), with a general westward displacement of the means from the oldest (late Olenekian, MES section data) to the youngest (late Ladinian, MEE section data) in the Botneheia Fm. (Fig. 11).

Magnetostratigraphic results

The fitted-line ChRM directions from Milne Edwardsfjellet were converted to virtual geomagnetic pole (VGP) latitudes using the fitted-line mean directions from each respective section (Table 1; Fig. 10c). For the specimens that had no fitted-line, the point on their great circle trend nearest the mean was used for calculating the VGP latitude (Fig. 10c). All specimens were also assigned a "polarity quality" (Fig. 10b), based on the quality of demagnetization behaviour, and, if from T-class specimens, the length and end-point position of the great circle trend (similar to the method used by Ogg & Steiner 1991; Hounslow, Hu et al. 2007). One specimen of good-quality polarity (i.e., S-type) was sufficient to define the horizon polarity, whereas with specimens of poorer quality, at least two were needed (Fig. 10d). Four horizons (one from the MES and three from the ME sections) failed to yield any specimens that could reliably be used to determine magnetic polarity (Fig. 10d).

The resulting horizon polarity through the two sections combined has resulted in a complex pattern of polarity changes (Fig. 10d). These have been numbered into 10 normal–reverse (N–R) couplets from the base of the MES section. The pattern of polarity changes is broken by substantive sampling gaps in the Vendomdalen Mb., whereas the more complete sampling through the Botneheia Fm. demonstrates that normal polarity dominates the lower 70 m of the formation, whereas reverse polarity dominates from this level upwards (Fig. 10d).

Discussion

The palaeomagnetic behaviour of the samples from the Vendomdalen Mb. at Milne Edwardsfjellet is not significantly different from that at Vikinghøgda, described by Hounslow et al. (2008). Both demonstrate that extraction of linear-trajectory, reverse polarity ChRMs from the demagnetization data is problematic. This is probably because of the nature of the magnetization carrier in the Vendomdalen Mb. (and also in the Botneheia Fm.), which appears to be of a mixed magnetite–sulphide magnetic mineralogy. Presumably, if the magnetic sulphide is early diagenetic in origin, the Triassic magnetization is

probably carried by both the magnetic sulphide and magnetite.

Comparison of the biomagnetostratigraphy in the Vendomdalen Mb., between Milne Edwardsfjellet and Vikinghøgda (Hounslow et al. 2008), demonstrates differences in the pattern of polarity changes, in part resulting from large changes in the sedimentation rate (Fig. 12). Some of these differences are compounded by the substantial sampling gaps. The reverse magnetozone MF1n.2r appears to be the equivalent of V8n.1r at Vikinghøgda, as both are immediately younger than the occurrence of *B. euomphala* in the sections. The midde part of the Vendomdalen Mb. is better characterized at Milne Edwardsfjellet than that at Vikinghøgda, where substantial sampling gaps occur, indicating that the early parts of the Keyserlingites subrobustus Zone are of mixed polarity (Fig. 12).

The uppermost part of the Vendomdalen Mb. and lowest Botneheia Fm. at Milne Edwardsfjellet is a dominantly reversed-polarity interval, whereas this same interval is of normal polarity at Vikinghøgda (Fig. 12). This suggests that there is a substantial hiatus near the Vendomdalen–Botneheia boundary at Vikinghøgda, where there is no representation of the equivalent of the MF2r or MF3 magnetozones (Fig. 12). The postulated hiatus does not violate the occurrence of *S. spitzbergensis*, which first occurs within the upper part of magnetozone MF2n, and at an equivalent interval at Vikinghøgda (Fig. 12). There is clear evidence of erosion of Permian deposits, indicated by the presence of the reworked palynomorphs *Vittatina* sp. and *Nuskoisporites* sp. some 2.5 m above the base of the Botneheia Fm. in the MES section—it seems probable that this level may represent the correlative disconformity at Milne Edwardsfjellet. The most likely correlative level between Vikinghøgda and Milne Edwardsfjellet in the base of the Botneheia Fm., is the *Rhizocorallium*-bearing siltstone, some 10 m above the base of the Botneheia Fm. at Vikinghøgda (Mørk, Elvebakk et al. 1999; Hounslow et al. 2008), which is the equivalent of the *Rhizocorallium*-bearing siltstone bed at the 30-m level in the ME section (Figs. 5, 12). These substantial magnetostratigraphic differences at the Vendomdalen–Botneheia boundary may have arisen because Vikinghøgda is close to the western side of the Ny Friesland Block (Fig. 2), and therefore may be more likely to have experienced minor Triassic uplift and erosion, associated with the Billefjorden basement fault complex.

Middle Triassic magnetostratigraphy tied to Tethyan and Boreal biostratigraphy

The distinctive feature of the lower part of the Botneheia Fm. is the dominance of normal polarity through magnetozones MF4n–MF7n. The Boreal ammonoids indicate an early to mid Anisian age for this interval. This appears to correspond to the dominantly normal-polarity interval (MT1n–MT4n) from near the base of the Anisian to the early Pelsonian in Tethyan successions (Fig. 12). Currently, a decision on the base Anisian global boundary stratotype and point (GSSP) has not been formally ratified, but the Desli Caira candidate section has been proposed, using either the first occurrence of the conodont *Chiosella timorensis* (Grădinaru et al. 2007) or the base of magnetozone MT1n (Hounslow, Szurlies et al. 2007; Figs. 12, 13) as the prime markers. Using the magnetostratigraphic correlations, either of these levels equates to within the lowest part of the Boreal Anisian (just above the base of the Grambergia taimyrensis Zone; Figs. 1, 12), following the earliest *Karangatites* sp. in the Boreal realm (Fig. 13). Correlation with the Polish Middle Triassic magnetostratigraphic data of Nawrocki & Szulc (2000) at this level is not directly constrained by any useful shared biostratigraphy, but the thicker and more complete succession through the central German Basin at this level (Szurlies 2007) shows a clear relationship with the Tethyan composite (Fig. 12). This is supported by an array of conodont and ammonite faunas in the middle and late Anisian parts of the Muschelkalk (Nawrocki & Szulc 2000; Szurlies 2007).

As a result of the high relative sedimentation rate in the lower part of the Botneheia Fm. (in the ME section), the lowest Anisian reverse magnetozones (i.e., MF4n.1r, MF4r and MF5r) are much expanded compared with both the Tethyan composite and with that in the Polish–German Basin (Fig. 12). The correlations proposed in Fig. 12 are supported by the occurrence of *Cs.* cf. *timorensis*, which ranges up through the MT3n magnetozone at the Kçira and Dęsli Caira sections (Muttoni et al. 1996; Grădinaru et al. 2007; Fig. 13).

Fig. 12 Other selected Late Olenekian and Middle Triassic biomagnetostratigraphies and probable correlations with the central Spitsbergen sections. The Vikinghøgda data are from Hounslow et al. (2008). The Tethys data are compiled from Muttoni et al. (2000), Muttoni et al. (2004), Grădinaru et al. (2007), Lehrmann et al. (2007), Orchard et al. (2007) and from the discussion in Hounslow, Szurlies et al. (2007). Magnetozones in the Alps column are numbered from the base to ease description in the text. Polish data are from Nawrocki & Szulc (2000), German composite data are from Szurlies (2007), with minor additional details, and Polish–German correlations are from Hounslow, Szurlies et al. (2007). The MEE section data are from Hounslow, Hu et al. (2007). S.s, *Svalbardiceras spitzbergensis*. The Olenekian–Anisian boundary interval is based on the Dęsli Caira section in Romania, with its two proposed boundary criteria (Grădinaru et al. 2007; Hounslow, Szurlies et al. 2007), neither of which has been formally ratified.

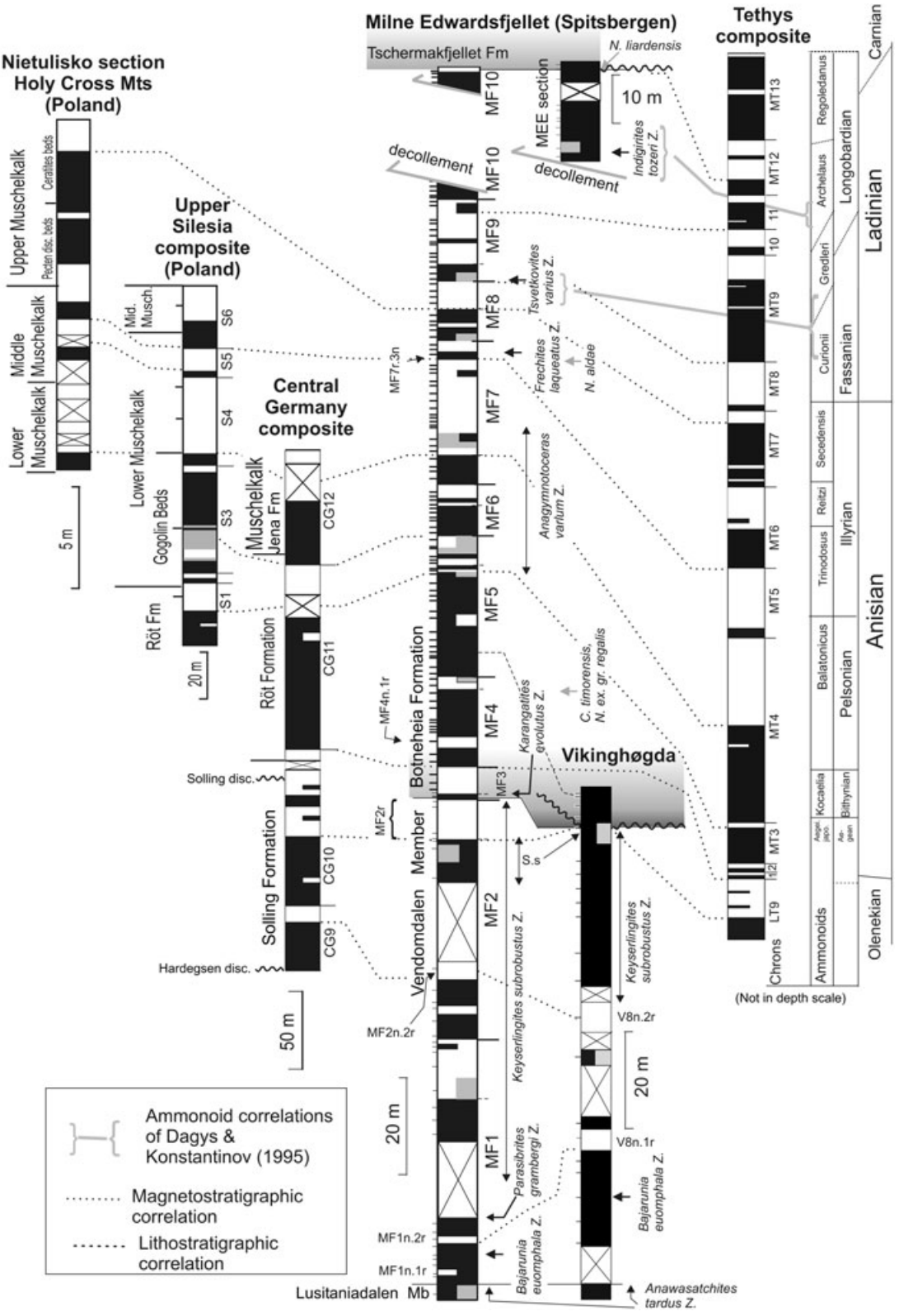
Nietulisko section
Holy Cross Mts
(Poland)
Upper Muschelkalk
Ceratites beds
Pecten disc. beds
Middle Muschelkalk
Lower Muschelkalk
5 m
Upper Silesia composite (Poland)
Mid. Musch.
Lower Muschelkalk
Gogolin Beds
Röt Fm
S6
S5
S4
S3
S1
20 m
Central Germany composite
Muschelkalk
Jena Fm
Röt Formation
CG12
CG11
CG10
CG9
Solling disc.
Solling Formation
Hardegsen disc.
50 m
Milne Edwardsfjellet (Spitsbergen)
Tschermakfjellet Fm
N. liardensis
MEE section
10 m
Indigirites tozeri Z.
decollement
decollement
MF10
MF9
MF8
MF7
MF6
MF5
MF4
MF3
MF2
MF1
Botneheia Formation
Member
Vendomdalen
Lusitaniadalen Mb
MF7r.3n
MF4n.1r
MF2r
MF2n.2r
MF1n.2r
MF1n.1r
Tsvetkovites varius Z.
Frechites laqueatus Z.
N. aldae
Anagymnotoceras varium Z.
C. timorensis,
N. ex. gr. regalis
Karangatites evolutus Z.
Vikinghøgda
S.s
Keyserlingites subrobustus Z.
Parasibirites grambergi Z.
Bajarunia euomphala Z.
Anawasatchites tardus Z.
V8n.2r
V8n.1r
20 m
20 m
Tethys composite
MT13
MT12
MT9
MT8
MT7
MT6
MT5
MT4
MT3
LT9
Chrons
Ammonoids
Regoledanus
Archelaus
Gredleri
Curionii
Secedensis
Reitzi
Trinodosus
Balatonicus
Kocaelia
Bithynian
Pelsonian
Illyrian
Fassanian
Longobardian
Carnian
Ladinian
Anisian
Olenekian
(Not in depth scale)
Ammonoid correlations of Dagys & Konstantinov (1995)
Magnetostratigraphic correlation
Lithostratigraphic correlation

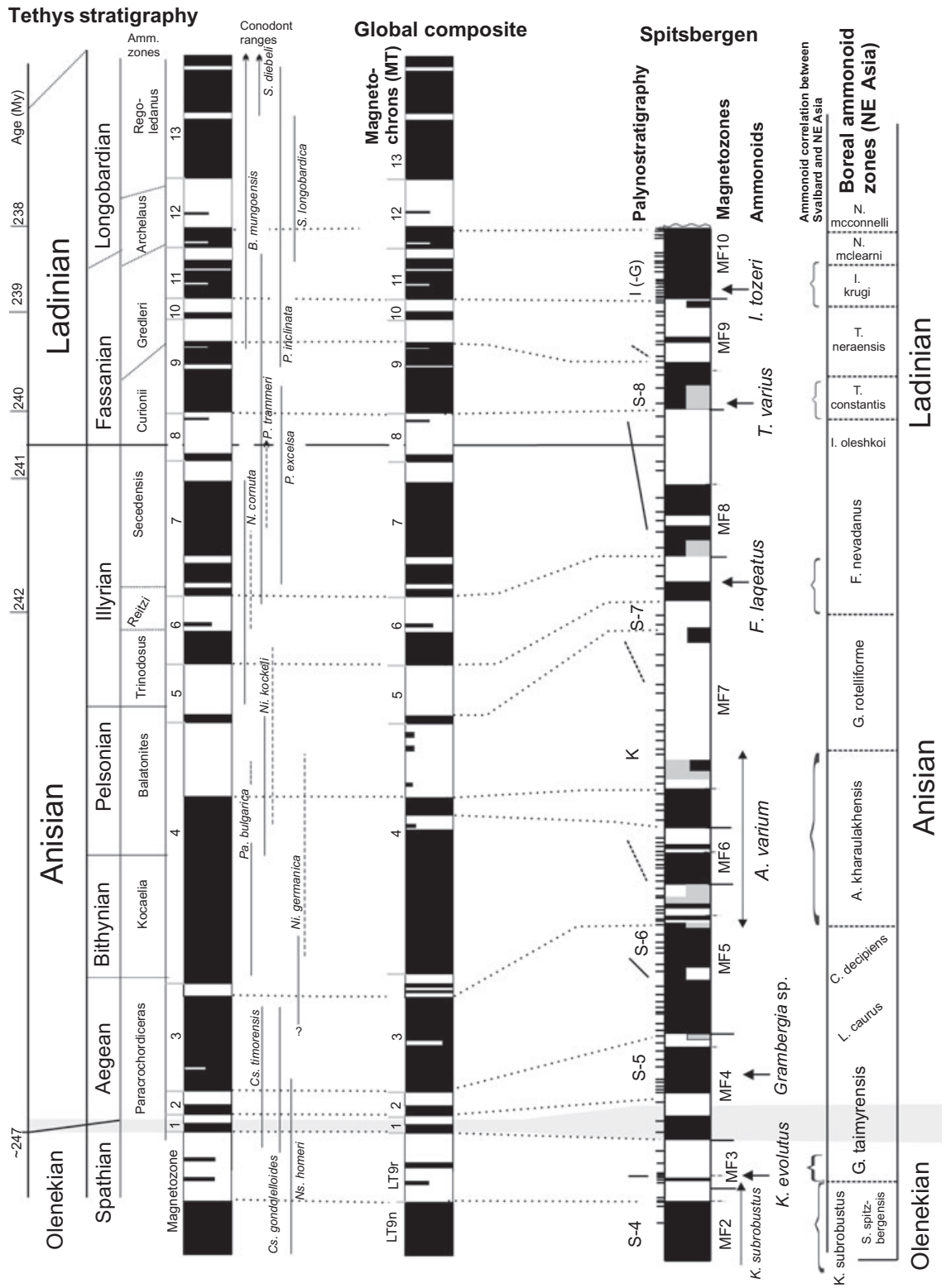
Tethys stratigraphy
Global composite
Spitsbergen
Age (My)
~247
238
239
240
241
242
Olenekian
Spathian
Aegean
Bithynian
Pelsonian
Illyrian
Fassanian
Longobardian
Anisian
Ladinian
Amm. zones
Rego-ledanus
Archelaus
Gredleri
Curionii
Secedensis
Reitzi
Trinodosus
Balatonites
Kocaelia
Paracrochordiceras
Conodont ranges
S. diebeli
B. mungoensis
S. longobardica
P. inclinata
P. trammeri
P. excelsa
N. cornuta
Ni. kockeli
Pa. bulgarica
Ni. germanica
Cs. timorensis
Cs. gondolelloides
Ns. homeri
Magnetozone
Magneto-chrons (MT)
LT9n
LT9r
Palynostratigraphy
Magnetozones
Ammonoids
S-4
S-5
S-6
K
S-7
S-8
I (-G)
MF2
MF3
MF4
MF5
MF6
MF7
MF8
MF9
MF10
K. subrobustus
K. evolutus
Grambergia sp.
A. varium
F. laqeatus
T. varius
I. tozeri
Ammonoid correlation between Svalbard and NE Asia
Boreal ammonoid zones (NE Asia)
K. subrobustus
S. spitz-bergensis
G. taimyrensis
C. decipiens
L. caurus
A. kharaulakhensis
G. rotelliforme
F. nevadanus
I. oleshkoi
T. constantis
T. neraensis
I. krugi
N. mclearni
N. mcconnelli
Olenekian
Anisian
Ladinian

Fig. 13 Composite global Middle Triassic magnetostratigraphy, and its correlation with the Boreal (north-east Asia) ammonoid time scale and the composite Tethyan magnetobiostratigraphy (Polish, German and Tethys sections in Fig. 12). Conodont range from the Muschelkalk sections in Fig. 12 are indicated by dashed lines; those from the Tethys composite are shown as solid. The Olenekian–Anisian boundary interval is shown in grey, based on the proposed criteria in the Dęsli Caira section (Grădinaru et al. 2007; Hounslow, Szurlies et al. 2007). Radiometric ages from Muttoni et al. (2004), Brack et al. (2005) and Lehrmann et al. (2007). Palynostratigraphy zones refer to Figs. 6 and 7. Dashed zone boundaries indicate an uncertain position of the base (or top). The Spitsbergen magnetostratigraphy has been arbitrarily stretched over the Anisian–Ladinian boundary interval, to provide a better visual fit to the global polarity time scale.

Magnetozone MF5r appears to equate to CG11r and interval S1r–S3n.1r in the Polish and German sections (Fig. 12), and also to a similarly-placed reverse magnetozone in the upper Guandao section in China (Orchard et al. 2007; Hounslow, Szurlies et al. 2007). The two single-horizon normal magnetozones within MF5r appear to be confirmed by the occurrence of two normal magnetozones at the correlated level in the Upper Silesia sections (i.e., S2n and S3n.1n; Fig. 12). The reverse magnetozone MF6r appears to be the equivalent to magnetozone S3r in the Polish Upper Silesia composite, which may also equate to a reverse magnetozone in both the lower and upper Guandao sections (Hounslow, Szurlies et al. 2007).

Above magnetozone MF7n is a dominantly reverse-polarity interval (MF7r–MF9r). The most important constraint that allows correlation with the Tethyan sections is the base of the Ladinian at Bagolino (the Ladinian GSSP), which is defined on the first occurrence of the genus *Eoprotrachyceras* (Brack et al. 2005). This level can be confidently correlated with the Eoprotrachyceras matutinium Zone (formerly known as the Eoprotrachyceras aspersum Zone; Orchard & Tozer 1997) of British Columbia, bearing the first representatives of the ammonoids Trachyceratidae (Dagys & Konstantinov 1995; Brack et al. 2005). In British Columbia the immediately younger T. poseidon Zone (formally known as the Progonoceras poseidon Zone; Orchard & Tozer 1997) contains *Arctoptychites* and forms related to *Tsvetkovites constantis*, allowing correlation with the T. constantis Zone of north-east Asia and the ammonite fauna of the Svalbard T. varius Zone (Fig. 1; Dagys & Weitschat 1993; Dagys & Konstantinov 1995). Together, these indicate that the base of the Ladinian is within the lower part of magnetozone MF8r (Figs. 12, 13), and that the magnetozone MF9n, which contains the T. varius Zone fauna, is the equivalent of the Tethyan magnetozone MT9n (Figs. 12, 13). On the assumption that there is no hiatus in the ME section between MF7r and MF8r, the most probable correlation with the Tethyan sections indicates MF8n is the equivalent of MT7n, and that MF7r.3n is the equivalent of MT6n (Fig. 12). The conodont *N. aldae* is a probable synonym of *Neogondolella cornuta*, which has been commonly identified in the Tethyan sections, ranging between MT5r and the top of MT7n (Fig. 13). This relationship generally confirms the magnetostratigraphic relationships proposed. However, other alternative correlations at this level are possible if a sequence boundary (and potential hiatus?) are hypothesized at this level, based on comparison with the Barents Sea, where a prominent sequence boundary characterizes the boundary between the Steinkobbe and Snadd formations, close to the boundary between the Svalis-7 and the Svalis-8 palynozones (Vigran et al. 1998; Fig. 13).

At least one normal magnetozone (i.e., MT5n) occurs within the dominantly reverse-polarity interval MT4r–MT5r, having been detected in the Polish Muschelkalk (magnetozone S5n in the Upper Silesia composite, and the probable equivalent in the Nietulisko section; Fig. 12). Sections at Granitivo and Nederlysaj in Bulgaria and Albania also display short-duration normal magnetozones at this level (Muttoni et al. 2000). Hounslow & McIntosh (2003) have also possibly detected two short-duration normal magnetozones at around this level. One or another of the putative normal magnetozones in the MF7r magnetozone may represent these intervals in the Milne Edwardsfjellet section.

At the Milne Edwardsfjellet ME section, the succession above MF9n is complicated by the décollement, and it is not certain how much of the section has been removed or repeated. Nevertheless, the continuous undisturbed MEE section through the uppermost part of the Botneheia Fm. indicates dominantly normal magnetic polarity to the top of the formation. This is supplemented by the uppermost undisturbed part across the Botneheia–Tschermakfjellet boundary in the ME section, which shows one horizon of reverse polarity (Figs. 10d, 12). We interpret the data from the overlapping ME and MEE sections as indicating one normal magnetozone (MF10n), with tentative evidence of an overlying magnetozone MF10r, from the single horizon highest in the Botneheia Fm. at the ME section. Following on from the lower part of the section, we would therefore suggest that MF9r is the equivalent of the combined MT9r and MT10, and that MF10n is the correlative of part or all of MT11 (or MT11–MT12n). The available biostratigraphic correlations seem to confirm this. Based on similarities and co-occurrences of

ammonoids between British Columbia, north-east Asia, Svalbard and the Alps, Dagys & Konstantinov (1995) suggest that the Svalbard I. tozeri Zone is approximately equivalent to the middle parts of the Protrachyceras archelaus Zone of the Alps (Gredleri and Archelaus Zones combined in Fig. 12). The fact that the conodont *N. liardensis* occurs in the top-most part of the Botneheia Fm. (in the MEE section), would suggest that the succession extends into beds equivalent to the F. sutherlandi Zone of British Columbia, which is equivalent to the Nathorstites mcconnelli Zone in north-east Asia (Dagys & Konstantinov 1995; Figs. 1, 13).

Palynostratigraphy comparisons

In combination with the palynology from the Spitsbergen sections, our data also provide additional detail on the age constraints of the palynological assemblage zones of Vigran et al. (1998). The ammonoid-derived ages of the Svalis Dome assemblages are generally similar to those indicated here, except for the Svalis-5 assemblage, which extends downwards into the very latest parts of the Olenekian. The data from the Svalis Dome cores are consistent with this, as the boundary between the Svalis-4 and Svalis-5 assemblages occurs in a 10-m interval, barren of ammonoids, between underlying occurrences of *Keyserlingites* sp. and overlying *Grambergia* sp. (Vigran et al. 1998).

The Svalis-8 assemblage may extend downwards into the latest Anisian, although the condensed sedimentation and wide sample spacing over this interval makes this conclusion less clear. Comparison of the Boreal palynological assemblages with well-dated (i.e., using conodonts and ammonoids) assemblages in lower latitudes is problematic, because there are few taxa in common (e.g., *J. punctispinosa*, *K. meieri*, *Dyupetalum vicentinence*, *Cyclotriletes triassicus* and *Aratisporites tenuispinosa*), and those that are shared, are only sporadically present (see Vigran et al. 1998; Kustatscher et al. 2006). Perhaps the simplest comparison is between the Svalis-8 assemblages with increased *Ovalipollis* sp. (*O. pseudoalatus* in the Svalis-8 assemblage) that characterize the transition into the Eoprotrachyceras curionii Zone in the Alps (Hochuli & Roghi 2002), which defines the base of the Ladinian (Brack et al. 2005; Fig. 13). The equivalence of these major palynological changes provides additional support for the placement of the base of the Ladinian in the ME section indicated in Figs. 12 and 13.

Conclusions

- The succession at Milne Edwardsfjellet provides a thick (ca. 110 m) and comparatively complete succession through the latest Spathian into the middle Anisian, whereas the late Anisian to Ladinian is comparatively condensed into about 70 m, with the latest Ladinian being absent (i.e., approximately younger than the Nathorstites mclearni Zone).
- The succession preserves a Triassic magnetostratigraphy, carried by magnetite and a magnetic sulphide, which is in part overprinted with a Brunhes-like magnetization.
- The mean magnetization directions demonstrate the close affinity to the early Mesozoic APWP of Baltica, demonstrating that the magnetization directions are primary.
- The high sedimentation rate through the latest Olenekian into the early Anisian allows a refinement of the magnetic polarity time scale over this interval.
- Discontinuous ammonoid and conodont recovery levels, assisted by palynostratigraphy, provide clear constraints for magnetostratigraphic correlation with biomagnetostratigraphies determined from lower latitudes. Age refinements of the Barents Sea regional palynostratigraphic zonation also result from this integrated stratigraphy.
- The base of the Anisian, informally defined in the Dęsli Caira section in Romania, maps onto an interval in the Boreal stratigraphy between the upper part of MF3r and the middle parts of MF4n.1r, equating to an interval within the Siberian Grambergia taimyrensis Zone.
- The base of the Ladinian in the Bagolino GSSP (Brack et al. 2005) maps closely onto the traditional base Ladinian (i.e., the base of the I. oleshkoi Zone) used in the Boreal realm.

Acknowledgements

Technical staff at IKU/SINTEF Petroleum Research and Lancaster (Simon Chew) helped with illustrations. The project was supported by Saga Petroleum ASA, Norsk Hydro ASA and Deminex. Morten Bergan and Rob Hawkins assisted in the field with palaeomagnetic sample collection. Valuable comments from Jerzy Nawrocki and Jim Ogg improved the manuscript. This is a contribution to IGCP project 467. The magnetostratigraphic data are archived in the MaGIC database.

References

Andresen A., Haremo P., Swensson E. & Bergh S.G. 1992. Structural geology around the southern termination of the Lomfjorden Fault Complex, Agardhdalen, east Spitsbergen. *Norsk Geologisk Tidsskrift 72*, 83–91.

Brack P., Riener H., Nicora A. & Mundil R. 2005. The global boundary stratotype and point (GSSP) of the Ladinian

Stage (Middle Triassic) at Bagolino (southern Alps, northern Italy) and its implication for the Triassic timescale. *Episodes 28*, 233–244.

Canfield D.E & Berner R.A. 1987. Dissolution and pyritization of magnetite in anoxic marine sediments. *Geochimica et Cosmochimica Acta 51*, 645–659.

Dagis A.A. 1984. Rannetriasovye konodonty severa Srednej Sibiri. (Early Triassic conodonts of northern Middle Siberia.) *Trudy Akademija SSSR, Sibirskoe otdelenie Instituta Geologii i Geofiziki 554*, 3–69.

Dagys A.S. & Konstantinov A.G. 1995. New zonation scheme of the Ladinian Stage for northeastern Asia. *Stratigraphy and Geological Correlation 3*, 121–127.

Dagys A.S. & Sobolev E.S. 1995. Parastratotype of the Olenekian Stage (Lower Triassic). *Albertiana 16*, 8–16.

Dagys A.S. & Weitschat W. 1993. Correlation of the Boreal Triassic. *Mitteilungen Geologisch-Paläontologisches Institut Universität Hamburg 75*, 249–256.

Dallmann W.K. (ed.) 1999. *Lithostratigraphic lexicon of Svalbard. Upper Palaeozoic to Quaternary bedrock. Review and recommendations for nomenclature use*. Tromsø: Norwegian Polar Institute.

Dekkers M.J., Passier H.F. & Schoonen M.A.A. 2000. Magnetic properties of hydrothermally synthesized greigite (Fe_3S_4)-II. High and low-temperature characteristics. *Geophysical Journal International 141*, 809–819.

Grădinaru E., Orchard M.J., Nicora A., Gallet Y., Besse J., Krystyn L., Sobolev E.S., Atudorei N.-V. & Ivanova D. 2007. The global boundary stratotype section and point (GSSP) for the base of the Anisian: Desli Caira Hill, North Dobregeo, Romania. *Albertiana 36*, 44–57.

Haremo P. & Andresen A. 1992. Tertiary décollement thrusting and inversion structures along Billefjorden and Lomfjorden Fault Zones, east central Spitsbergen. In R.M. Larsen et al. (eds.): *Structural and tectonic modelling and its application to petroleum geology*. Pp. 481–494. Amsterdam: Elsevier.

Hochuli P.A., Colin J.P. & Vigran J.O. 1989. Triassic biostratigraphy of the Barents Sea area. In J.D.Collinson (ed.): *Correlation in hydrocarbon exploration*. Pp. 131–153. London: Graham & Trotman.

Hochuli P.A. & Roghi G. 2002. A palynological review of the Anisian–Ladinian boundary—new results from the Seceda section (Dolomites, northern Italy). *Abstract volume of the STS/IGCP 467 Field Meeting, Veszprem, Hungary, 5–8 September 2002*. Pp. 29–30. Budapest: Geological Institute of Hungary.

Hounslow M.W., Hu M., Mørk A., Vigran J.O., Weitschat W. & Orchard M.J. 2007. Magneto-biostratigraphy of the lower part of the Kapp Toscana Group (Carnian), Vendomdalen, central Spitsbergen, Arctic Norway. *Journal of the Geological Society, London 164*, 581–597.

Hounslow M.W. & McIntosh G. 2003. Magnetostratigraphy of the Sherwood Sandstone Group (Lower and Middle Triassic), south Devon, UK: detailed correlation of the marine and non-marine Anisian. *Palaeogeography, Palaeoclimatology, Palaeoecology 193*, 325–348.

Hounslow M.W., Peters C., Mørk A., Weitschat W. & Vigran J.O. 2008. Bio-magnetostratigraphy of the Vikinghøgda Formation, Svalbard (Arctic Norway), and the geomagnetic polarity timescale for the Lower Triassic. *Geological Society of America Bulletin 120*, 1305–1325.

Hounslow M.W., Szurlies M., Muttoni G. & Nawrocki J. 2007. The magnetostratigraphy of the Olenekian–Anisian boundary and a proposal to define the base of the Anisian using a magnetozone datum. *Albertiana 36*, 62–67.

Hunt C.P., Moskowitz B.M. & Banerjee S.K. 1995. The magnetic properties of rocks and minerals. In T.J. Ahrens (ed.): *Global earth physics. Handbook of physical constants*. Pp. 189–204. Boston: American Geophysical Union.

Kent J.T., Briden J.C. & Mardia K.V. 1983. Linear and planar structure in ordered multivariate data as applied to progressive demagnetisation of palaeomagnetic remanence. *Geophysics Journal of the Royal Astronomical Society 81*, 75–87.

King J.G. & Williams W. 2000. Low temperature magnetic properties of magnetite. *Journal of Geophysical Research—Solid Earth 105*, 16427–16436.

Klets T.V. 1998. Novye vidy konodontov iz Nižnego Triasa Kolymskogo Bassejna. (New species of conodonts from the Lower Triassic of the Kolyma Basin.) *News of Paleontology and Stratigraphy. Supplement to Geologija i Geofizika 39*, 113–121.

Kustatscher E., Manfrin S., Mietto P., Posenato R. & Roghi G. 2006. New biostratigraphic data on Anisian (Middle Triassic) palynomorphs from the Dolomites. *Review of Palaeobotany and Palynology 140*, 79–90.

Lehrmann D.J, Ramezani J., Bowring S.A., Martin M.W., Montgomery, P., Enos P., Payne J.L., Orchard M.J., Hongmei W. & Jiayong W. 2007. Timing of recovery from the end-Permian extinction: geochronologic and biostratigraphic constraints from south China. *Geology 34*, 1053–1056.

Lowrie W. 1990. Identification of ferromagnetic minerals in a rock by coercivity and unblocking temperature profiles. *Geophysical Research Letters 17*, 159–162.

McFadden P.L. & McElhinney M.W. 1988. The combined analysis of remagnetisation circles and direct observations in palaeomagnetism. *Earth and Planetary Science Letters 87*, 161–172.

McFadden P.L. & McElhinney M.W. 1990. Classification of the reversal test in palaeomagnetism. *Geophysical Journal International 103*, 725–729.

Muttoni G., Gaetani M., Budurov K., Zagorchev I., Trifonova E., Ivanova D., Petrunova L. & Lowrie W. 2000. Middle Triassic palaeomagnetic data from northern Bulgaria: constraints on Tethyan magnetostratigraphy and palaeogeography. *Palaeogeography Palaeoclimatology Palaeoecology 160*, 223–237.

Muttoni G., Kent D.V., Meço S., Balini M., Nicora A., Rettori R., Gaetani M. & Krystyn L. 1998. Towards a better definition of the Middle Triassic magnetostratigraphy and biostratigraphy in the Tethyan realm. *Earth and Planetary Science Letters 164*, 285–302.

Muttoni G., Kent D.V., Meço S., Nicora A., Gaetani M., Balini M., Germani D. & Rettori R. 1996. Magnetobiostratigraphy of the Spathian to Anisian (Lower to Middle Triassic) Kçira section, Albania. *Geophysical Journal International 127*, 503–514.

Muttoni G., Nicora A. M., Brack P. & Kent D.V. 2004. Integrated Anisian–Ladinian boundary chronology. *Palaeogeography, Palaeoclimatology, Palaeoecology 208*, 85–102.

Mørk A., Dallmann W.K., Dypvik H., Johannessen E.P., Larssen G.B., Nagy J., Nøttvedt A., Olaussen S., Pchelina T.M. & Worsley D. 1999. Mesozoic lithostratigraphy. In W.K. Dallmann (ed.): *Lithostratigraphic lexicon of Svalbard. Upper Palaeozoic to Quaternary bedrock. Review and recommendations for nomenclature use*. Pp. 127–214. Tromsø: Norwegian Polar Institute.

Mørk A., Elvebakk G., Forsberg A.W, Hounslow M.W., Nakrem H.A., Vigran J.O. & Weitschat W. 1999. The type section of the Vikinghøgda Formation: a new Lower Triassic unit in central and eastern Svalbard. *Polar Research 18*, 51–82.

Mørk A., Vigran J.O., Korchinskaya M.V., Pchelina T.M., Fefilova L.A., Vavilov M.N. & Weitschat W. 1992. Triassic rocks in Svalbard, the Arctic Soviet islands and the Barents Shelf: bearing on their correlations. In T.O. Vorren et al. (eds.): *Arctic geology and petroleum potential: proceedings of the Norwegian Petroleum Society Conference, 15–17 August 1990, Tromsø, Norway*. Pp. 457–479. Amsterdam: Elsevier.

Nakrem H.A, Orchard M.J., Weitschat W., Hounslow M.W., Beatty T.W. & Mørk A. 2008. Triassic conodonts from Svalbard and their Boreal correlations. *Polar Research 27*, 523–539.

Nawrocki J. & Szulc J. 2000. The Middle Triassic magnetostratigraphy from the Peri-Tethys basin in Poland. *Earth Planetary Science Letters 182*, 77–92.

Ogg J.G. & Steiner M.B. 1991. Early Triassic polarity time-scale: integration of magnetostratigraphy, ammonite zonation and sequence stratigraphy from stratotype sections (Canadian Arctic Archipelago). *Earth Planetary Science Letters 107*, 69–89.

Orchard M.J. 2007. New conodonts and zonation, Ladinian–Carnian boundary beds, British Columbia, Canada. *New Mexico Museum of Natural History and Science Bulletin 41*, 321–330.

Orchard M.J., Grădinaru E. & Nicora A. 2007. A summary of the conodont succession around the Olenekian–Anisian boundary at Deşli Caira, Dobrogea, Romania. *New Mexico Museum of Natural History and Science Bulletin 41*, 341–346.

Orchard M.J. & Tozer E.T. 1997. Triassic conodont biochronology, its calibration with the ammonoid standard and a biostratigraphic summary for the western Canada sedimentary basin. *Bulletin of Canadian Petroleum Geology 45*, 675–692.

Rochette P., Jackson M. & Auboug C. 1992. Rock magnetism and the interpretation of anisotropy of magnetic susceptibility. *Reviews in Geophysics 30*, 209–226.

Sweet W.C. 1970. Uppermost Permian and Lower Triassic conodonts of the Salt Range and Trans-Indus Ranges, west Pakistan. In B. Kummel & C. Teichert (eds.): *Stratigraphic boundary problems: Permian and Triassic of west Pakistan*. Pp. 207–275. Lawrence, KS: University of Kansas Press.

Szurlies M. 2007. Latest Permian to Middle Triassic cyclo-magnetostratigraphy from the Central European Basin, Germany: implications for the geomagnetic polarity timescale. *Earth and Planetary Science Letters 261*, 602–619.

Torsvik T.H. & Cocks L.R.M. 2005. Norway in space and time: a centennial cavalcade. *Norwegian Journal of Geology 85*, 73–86.

Tozer E.T. 1994. *Canadian Triassic ammonoid faunas. Geological Survey of Canada Bulletin 467*. Ottawa: Geological Survey of Canada.

Vigran J.O., Mangerud G., Mørk A., Bugge T. & Weitschat W. 1998. Biostratigraphy and sequence stratigraphy of the Lower and Middle Triassic deposits from the Svalis Dome, central Barents Sea, Norway. *Palynology 22*, 89–141.

Weitschat W. & Dagys A.S. 1989. Triassic biostratigraphy of Svalbard and a comparison with NE-Siberia. *Mitteilungen Geologisch-Paläontologisches Institut Universität Hamburg 68*, 179–213.